

Balancing and Frequency Control of Power systems in Presence of Wind Farms and Utility-Scale Power-to-Hydrogen Plants

Basel Assaf Salman
Energy Technology, WPS4-1052, 2022

Master Thesis



Copyright © Aalborg University 2022

Here you can write something about which tools and software you have used for typesetting the document, running simulations and creating figures. If you do not know what to write, either leave this page blank or have a look at the colophon in some of your books.



AAU Energy
Aalborg University
<http://www.aau.dk>

AALBORG UNIVERSITY

STUDENT REPORT

Title:

Balancing and Frequency Control of Power systems in Presence of Wind Farms and Utility-Scale Power-to-Hydrogen Plants

Theme:

Master Thesis Report

Project Period:

Autumn Semester 2022

Project Group:

WPS4 - 1052

Participant(s):

Basel Assaf Salman

Supervisor(s):

Amjad Anvari-Moghaddam

Page Numbers: 56

Date of Completion:

October 14, 2022

Abstract:

The increasing tendency of integrating more Renewable Energy Sources (RES) into the utility grid in Denmark, is due to the goals set by the country as stated in 2030 and 2050 plans. Denmark relies mainly on Wind power plants to achieve the transition to green energy-based systems. In order to overcome the challenges associated with the power fluctuation of wind power plants that might compromise the frequency stability of the grid, energy storage has become a potential solution like power-to-X, especially power-to-hydrogen technology. The aim of this paper is to develop a control method for a wind power plant combined with a power-to-hydrogen unit, an electrolyzer, and a fuel cell stack to mitigate frequency deviation and balance the power system. After developing a model of the power system in Matlab/Simulink platform, the performance of the system is investigated and has shown that the implemented control algorithm has managed to balance the power system and control the frequency with the help of the electrolyzer and the fuel cell stack.

The content of this report is freely available, but publication (with reference) may only be pursued due to agreement with the author.

By accepting the request from the fellow student who uploads the study group's project report in Digital Exam System, you confirm that all group members have participated in the project work, and thereby all members are collectively liable for the contents of the report. Furthermore, all group members confirm that the report does not include plagiarism.

Summary

As Denmark increases its electrical grid penetration level of wind power plants in order to realize its 2030 and 2050 plans, rises the necessity of mitigating the power disturbance due to the wind speed dependant power production of wind power plants.

This master's thesis covers the studies of utilizing power-to-X (power-to-hydrogen), aka water electrolysis technology as energy storage to power a fuel cell stack to aid a wind power plant in contributing to the balance and frequency control of a power system by the use of a developed control algorithm.

The control algorithm aims to mitigate frequency deviations caused by power production fluctuations of the wind power plant and when the power system undergoes sudden load changes, i.e. connecting and disconnecting loads.

The components of the proposed power system are presented and modeled in Matlab/Simulink platform.

Assessment study, in which the contribution of the electrolyzer and the fuel cell stack, shows that the control algorithm achieves satisfactory results in terms of frequency control and maintaining the power balance.

Preface

This Master's project is conducted by the group WPS4-1052 from the 10th semester at Aalborg University as a part of the Wind Power Systems master program. The title of the project is *Balancing and Frequency Control of Power systems in Presence of Wind Farms and Utility-Scale Power-to-Hydrogen Plants*.

The author would like to give a special thanks to the supervisor *Amjad Anvari-Moghaddam* for guidance and huge support during the project.

Readers guide

Figures and tables in the report are denoted according to the respective chapter. In this way the first figure in chapter 2 is defined as 2.1, the number of the second figure will be 2.2, and so on. Explanatory text is found under the given figures and tables. Figures without reference are made by the project group.

On page **xi**, a Table of Contents is given. When viewing this report as a PDF, hyperlinks in the table of contents will allow fast navigation to the desired sections. Additionally, a table of figures is found on page **xiii** in order to find the actual place of the figure quickly.

The bibliography can be found on page 39 and is sorted after their order of appearance in the text. All the appendices can be found after the bibliography, which are labeled with letters.

If a source is used to cite a specific piece of information, the source will appear before the period [source no.]. If a source is used in general in the entire paragraph, it will appear after the period at the end of the paragraph. [source no.]

Aalborg University, October 14, 2022

Basel Assaf Salman
<bsalma16@student.aau.dk>

Contents

List of Figures	xiii
1 Introduction	1
1.1 Background and Motivation	1
1.2 State of the art	3
1.3 Problem Statement	5
1.3.1 Objectives	5
1.3.2 Limitations	5
1.3.3 Methodology	6
1.4 Summary	6
2 System Description	7
2.1 Wind Power Plant	8
2.2 Electrolyzer Unit	9
2.3 Fuel cell Stack Unit	10
2.4 Load	11
2.5 Utility grid	11
2.6 Summary	12
3 Modeling and Model Verification	13
3.1 Modelling	13
3.1.1 Wind Power Plant	13
3.1.2 Electrolyzer plant	14
3.1.3 Fuel cell model	17
3.1.4 Buck converter	18
3.2 Model Verification	19
3.3 Summary	25
4 Assessment Studies	27
4.1 Case study	27
4.2 Summary	33

5 Conclusion and Future work	35
5.1 Conclusion	35
5.2 Future work and Recommendations	36
Bibliography	39
A Appendix A	43
B Appendix B	49
C Appendix C	53

List of Figures

1.1	Worldwide increase of renewable electricity generation between 2019 and 2021 [1]	1
1.2	Technologies share in electricity production in Denmark [2]	2
2.1	Single line diagram of the proposed power system	8
2.2	Block diagram of a DFIG-based wind turbine	9
2.3	Visualization of the operating principle of a single cell PEM electrolyzer and hydrogen production, inspired by [3]	10
2.4	Single line diagram showing possible topologies used in fuel cell unit application related to dc- and ac connection	11
2.5	Single line diagram of the utility grid	12
3.1	Block diagram showing the implementation of the aerodynamic part	14
3.2	Layout of an equivalent electrical model of a PEM electrolyzer, inspired by [4]	15
3.3	Block diagram showing the implementation of the PEM electrolyzer	17
3.4	Single line diagram of a converter/ inverter	17
3.5	Block diagram of the current control loop	18
3.6	Topology of buck converter	18
3.7	Verification of the wind power plant model	20
3.8	Voltage and current profiles at the converter powering the electrolyzer	21
3.9	Active and reactive power supplied to the electrolyzer, and the dc-input voltage of the electrolyzer	22
3.10	State of charge of the hydrogen tank and the produced hydrogen flow rate	23
3.11	Voltage and current profiles of the fuel cell stack during performed switchings	24
3.12	Active and reactive power profiles exchanged by the fuel cell system	25
4.1	Flow chart of the developed control algorithm	28
4.2	Voltage and current profiles measured at the point of connection . .	29
4.3	Power profile of the power generating and consuming units	30

4.4	Voltage and current behavior measured at the converter powering the electrolyzer	31
4.5	Voltage and current profiles measured at the inverter supplied by the fuel cell stack	32
4.6	Frequency profile during the simulation	33
A.1	VI-characteristics of a single PEM cell	47
B.1	Power profiles	49
B.2	Frequency behavior	50
B.3	Power profiles	51
B.4	Frequency behavior	52
C.1	Total system implementation in OPAL-RT	54
C.2	Structure of the implemented system in OPAL-RT	55
C.3	Monitoring block and data acquisition in OPAL-RT	56

Nomenclature

Acronyms

AC	Alternating Current
DC	Direct Current
DFIG	Doubly Fed Induction Generator
FC	Fuel Cell
HV	High Voltage
K	Gain (Constant)
LV	Low Voltage
PEM	Polymer electrolyte membrane
PID	Proportional, Integrator and Derivative
pu	Per-Unit
SoA	State of the Art
S.S	Steady-State
T	Transformer

Variables

Symbol	Description	Unit
C	Capacitance	F
f	Frequency	Hz
I	Current	A
L	Inductance	H
N_s	Shaft Speed	rpm
P	Active Power	W
Q	Reactive Power	VAr
S	Apparent Power	VA
t	Time	s
V	Voltage	V
ω	Angular Velocity	Rad/s
ϕ	Flux	Web
τ	Torque	Nm

Chapter 1

Introduction

This chapter provides the reader with an introduction to establish a background for the increasing trend of integrating wind power plants and their potential challenges that can impact the power system in case of high penetration levels. Additionally, this chapter introduces potential solutions that might contribute to grid support, particularly frequency control and power balance. Lastly, this chapter presents the problem formulation and a set of objectives to be met in this project work.

1.1 Background and Motivation

Environmental and energy security (crisis) considerations have led many countries around the world to invest in research for alternative energy resources in order to minimize the dependency on fossil fuel-based power plants [5]. The growth of renewables and their additional contribution to the electricity generation sector between 2019 and 2021 over the globe is shown in Figure 1.1

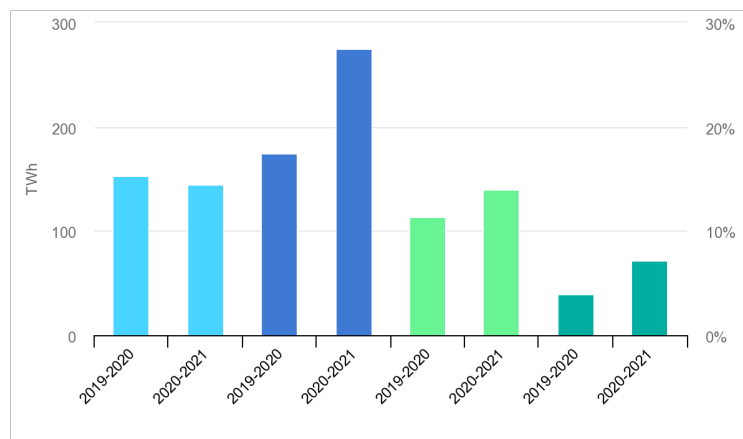


Figure 1.1: Worldwide increase of renewable electricity generation between 2019 and 2021 [1]

Figure 1.1, illustrates the installed capacity and the growth of different renewable energy-based technologies, like light blue, represents photovoltaic plants, navy blue describes the expansion of wind energy, light green depicts the growth of hydro-based energy and dark green illustrates the increased incorporation of bioenergy in the electricity generation sector.

Countries like Denmark for example have conducted a set of plans, which were triggered by the energy crisis in the 1970s, where it aims to supply 55% of its demand by renewable energy resources, which is known as the 2030-plan. Additionally, Denmark aims to reduce its CO₂ footprint, even more, to be 100% free of fossil fuel dependence by 2050. [6]

Similar to its counterparts, the growth of wind energy in Denmark is the highest amongst the other renewable energy-based technologies, due to its geographical location and its leading position in researching in this technology. This is illustrated in Figure 1.2.

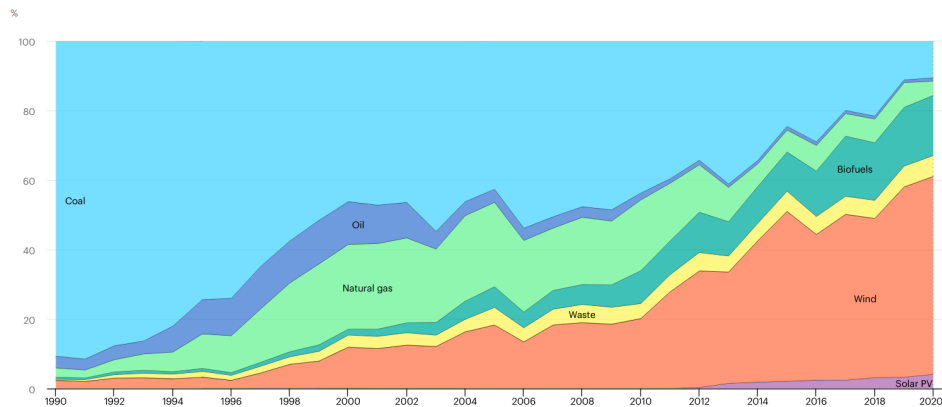


Figure 1.2: Technologies share in electricity production in Denmark [2]

Figure 1.2, shows that wind energy contribution in the electricity generation sector has exceeded 60% just before the year 2020. Wind energy conversion technology has undergone lots of improvements over the years. [7] Wind Energy Conversion Systems (WECS) have two types: Variable Speed Wind Turbines (VSWTs) and Fixed Speed Wind Turbines (FSWTs) based on their behavior under variable wind speeds. The former type is the more dominating type in terms of growth due to its characteristics in terms of controllability and maximum power extraction aspects. [8] Furthermore, wind turbines can be categorized into 4 major commercial types based on the type of the implemented generator. The most common types are type 3 and type 4, where type 3 utilizes a Doubly-Fed Induction Generator (DFIG), and type 4 uses a variety of Synchronous Generator types eg. a Permanent Magnet Synchronous Generator (PMSG). [9]

However, the varying behavior of the wind may present challenges for increasing the wind energy penetration level for the power system. These challenges affect the stability of the power system, which has led to introducing requirements, i.e. grid codes to be fulfilled by the modern wind power plants.[10] One of the major challenges of the high level of wind energy integration in a power system is the compensation for the fluctuation in active power and thereby system frequency, which requires power reserve either by energy storage systems or as commonly used conventional power plants in order to ensure the control and stability by performing generation- load balancing process. The integration of wind energy affects the power system inertia, as the modern wind turbines are decoupled from the grid by power converters, i.e. systems inertia reduces as the penetration level increases. [11] This will lead to a more frequency-sensitive power system due to forecasting errors as the conventional power plants are dispatched, and less response time is allocated to the remaining conventional power plant to stabilize the frequency. [12] Therefore, it is interesting to investigate solutions for future power systems with a high RES participation level.

1.2 State of the art

Various types of research are conducted for utilizing the capabilities of (VSWTs) on a plant level to optimize the power production by the plant in order to satisfy the frequency stability of the system by controlling the rotor speed. the downside with this approach is the potential losses in wind power as the turbine will not operate at its maximum power point in order to provide a power reserve.[13] Secondary control can be utilized in order to restore the frequency set-point by adjusting the injected active power to match the load demand, as the primary control reduces the imbalance in the system frequency. However, the secondary control shall be notified 15 minutes in advance. [14]

Wind power generating units can be accommodated with energy storage systems like BESS, ultracapacitors, etc. [15] The energy storage systems can smooth the dynamics of the power system caused by the non-dispatchable generation units. [16]

Recently, power-to-X technology is being heavily researched and investigated to serve as an energy storage system that can potentially contribute to mitigating the challenges associated with a higher level of renewable energy-based sources penetrating the grid, e.g. power-to-hydrogen. Power-to-hydrogen is considered a promising candidate for its storage capacity, and capability to provide grid support and the produced hydrogen can potentially be utilized in the heating-, and transport sectors. [17]

According to the danish energy agency, power-to-hydrogen would play an important role to realize both 2030 and 2050 plans. [18]

This paper adopts standards defined as grid requirements for grid-connected type-B wind power plant and energy storage systems set by the danish TSO Energinet as illustrated in Table 1.1. [19]

Frequency band	DK1	DK2
Hz	49.8-50.2	49.9-50.1

Table 1.1: Frequency band for the grid-connection operating mode.

In Table 1.1, DK1 refers to the electrical grid covering Western Denmark, which is synchronized with the European grid. Dk2 refers to the electrical grid covering Eastern Denmark that is synchronized with the other Nordic countries' grids.

1.3 Problem Statement

The thesis statement and its corresponding objectives will be presented in the section based on the background and motivation in order to address the challenges related to the rising trend in wind energy integration level in the power system by the use of power-to-X technology and utilizing the green hydrogen to power a fuel cell stack.

How to maintain the power balance and provide frequency support of a type-B wind power plant combined with a power-to-hydrogen storage system and a fuel cell stack in an electrical power system?

1.3.1 Objectives

- To develop a detailed model of a DFIG-based wind turbine in order to assess the frequency stability of the total system.
- To develop a model of the power-to-X system comprising an electrolyzer and its converter.
- To implement a fuel cell model to contribute to power production and demand matching.
- To implement a control algorithm for coordinating the green hydrogen production and consumption by the electrolyzer and the fuel cell stack, respectively.
- To conduct sensitivity analysis by carrying out an assessment study to evaluate the performance of the proposed control strategy with respect to the grid code requirements.

1.3.2 Limitations

The limitations are considered in this thesis to narrow the scope of the framework to satisfy the study curriculum and the allocated time for the thesis. The limitations are listed as follows:

- The wind power plant will consist of a single wind turbine.
- A voltage source will be implemented serving as a fuel cell stack assuming available hydrogen on demand and constant voltage after the boosting stage of the voltage.
- Frequency behavior of the system at PCC will be the main focus of this thesis.

- Voltage quality will not be captured in this thesis.
- Forecasting of the estimated power production and load demand will not be considered in this thesis.
- The economical evaluation will not be a part of the assessment studies in the framework of the thesis.

1.3.3 Methodology

Chapter 1 includes a motivational introduction and a state of the art to provide a background to introduce a problem statement. Objectives are also included to pave the way to propose a solution for the problem statement and to fulfill the goal of the thesis.

The power system components will be described in Chapter 2.

A model of the proposed power system will be implemented in Simulink[®] to validate the model and conduct sensitivity analysis in Chapters 3 and 4, respectively.

The modeling approach will be based on modeling each component of the system and verifying its performance individually before assembling the total system in Simulink[®] platform, and the data acquired by the simulations are processed using MATLAB[®].

Chapter 5 includes the thesis's conclusion and future work.

Appendices will contain additional relevant information.

1.4 Summary

Chapter 1 has presented the background and a motivational introduction to the potential impact of increasing the penetration level of wind power plants on the frequency stability of power systems and the potential technologies that could contribute to frequency support. Additionally, this chapter has included a thesis statement, objectives, limitations, and methodology of the framework that would be expected in this thesis.

Chapter 2

System Description

This chapter provides the reader with a description of the proposed system comprising a Wind power plant, Electrolyzer, and grid-connected Fuel cell stack module, whose impact on grid stabilization is to be investigated.

Proposed System

The proposed system, adopted in this thesis to conduct assessment studies for a power-to-X system, consists of a 1.5 MW type 3 wind turbine operating in grid-connected mode. At the point of common coupling (PCC), an electrolyzer system is connected to the same busbar. Additionally, a fuel cell stack system is connected to the PCC, where a varying load demand with a maximum demand of 1.6 MW is to be supplied by the wind power plant and the utility grid. The total system is illustrated in Figure 2.1. The aim of utilizing the electrolyzer system is to produce green energy-based hydrogen that can supply hydrogen tank stations or fuel cell stack units, which both can inject electrical power back into the grid or connect the electrolyzer to mitigate the impact of disconnecting a load suddenly for stabilizing power production and load demand balance.

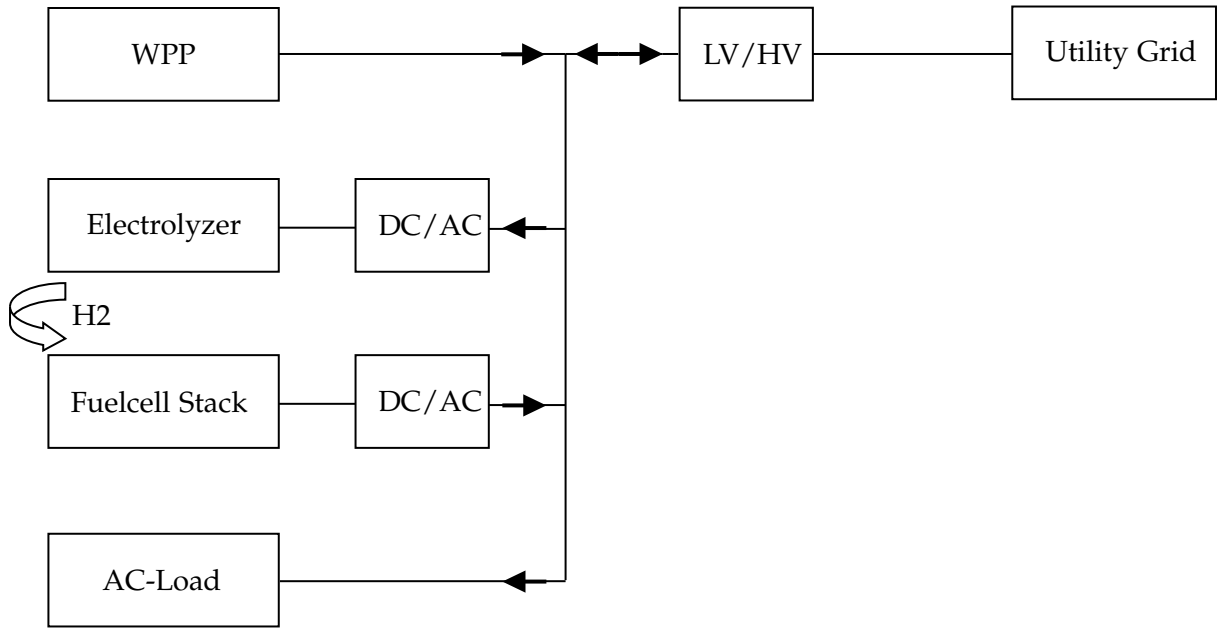


Figure 2.1: Single line diagram of the proposed power system

The wind power plant is connected to the grid as seen in Figure 2.1. It injects the produced electricity into the grid through a step-up transformer and a 20 km line after which a step-down transformer is used to supply a low voltage level distribution grid.

The components of the total systems are described in the following sections.

2.1 Wind Power Plant

The wind power plant consists of a 1.5 MW type-3 wind turbine adopting a Doubly-fed Induction based Generator (DFIG) topology. The aerodynamic part of the turbine captures the kinetic energy of the wind and transfers this energy into rotating mechanical energy. The shaft speed is increased to the operating angular speed range by a gearbox, whose high-speed side is connected to the generator. One of the most significant advantages of type-3 wind turbines is the smaller size of their converter compared to their counterparts like the converters implemented in type-4 wind turbines, which are based on Synchronous Generators (SG). The stator of the generator is directly connected to the grid, where the rotor is connected to the grid by a back-to-back converter. [20]

A typical structure of the type-3 wind turbine is depicted in Figure 2.2.

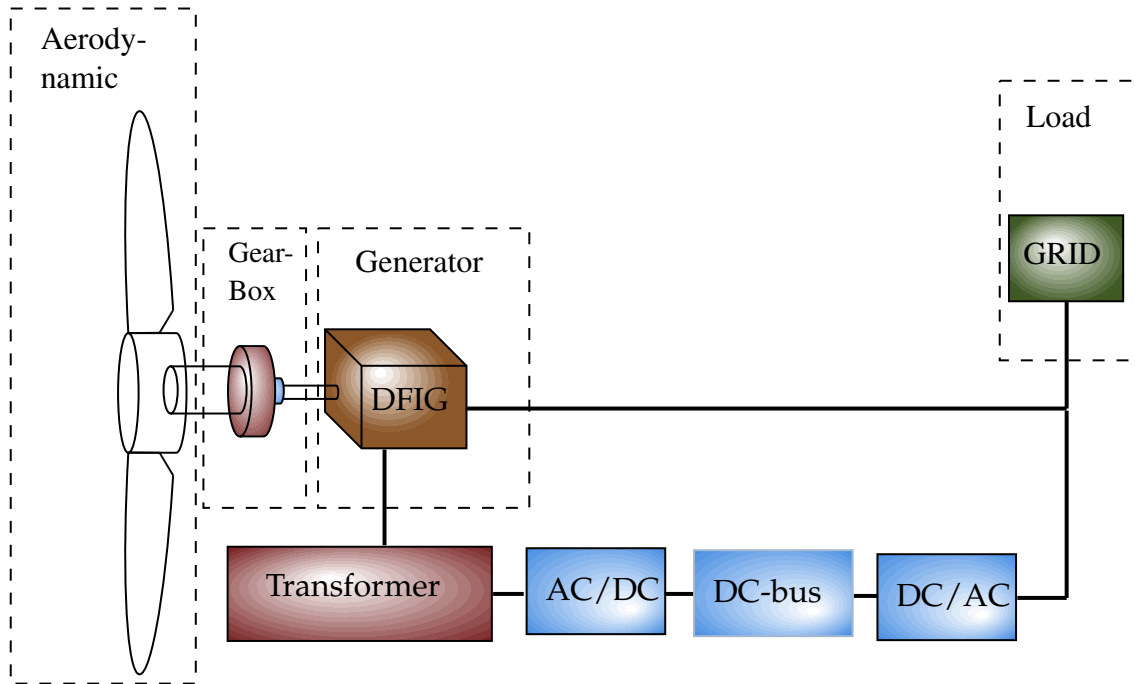
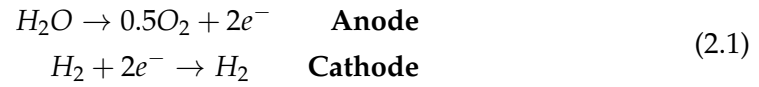


Figure 2.2: Block diagram of a DFIG-based wind turbine

2.2 Electrolyzer Unit

An electrolyzer system is the main unit in any power-to-X system, which can operate as an energy storage system by its electrolysis process, in which the water is split into hydrogen and oxygen. The produced hydrogen can be stored and utilized in the transport sector, heating sector, and re-electrification through fuel cell modules. There are three major types of commercially available electrolyzers, namely Alkaline electrolyzers, Polymer Electrolyte Membrane (PEM) electrolyzers, and Solid Oxide Electrolysis (SOEC) electrolyzers. The main differences between each type are current density, operating temperature, dynamic response, and system efficiency. PEM electrolyzer system operates at a low temperature similar to an alkaline system, however, its response time is faster than the alkaline unit. Additionally, the efficiency of a PEM electrolyzer is slightly higher than an alkaline unit. The SOEC electrolyzer operates at high temperatures between 650- 1000 C, with the highest efficiency among the other two types. The dynamic response time of the SOEC is also comparable to the PEM modules. The electrolysis process of a PEM unit is described in Equation 2.1. [3]



The electrolysis process in Equation 2.1 is visualized in Figure 2.3.

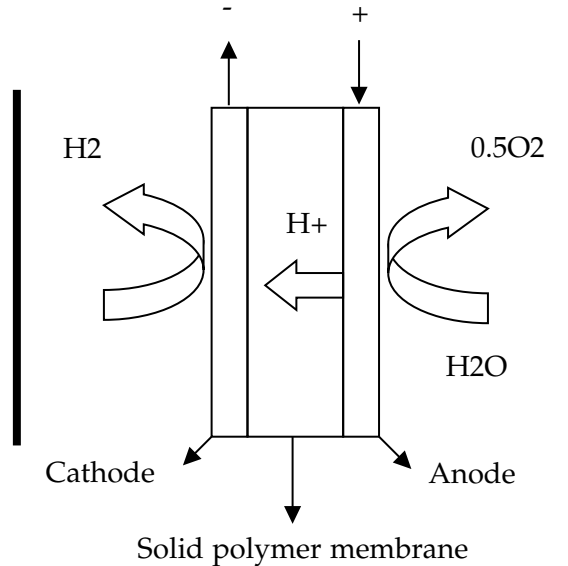


Figure 2.3: Visualization of the operating principle of a single cell PEM electrolyzer and hydrogen production, inspired by [3]

In Figure 2.3, the water feeding the PEM unit enters the anode inlet where the oxygen is separated at the anode side and the hydrogen leaves the unit from the cathode outlet. Additionally, the anode is connected to the positive side of the dc electrical power supply, and the cathode is connected to the negative side. The produced hydrogen is stored in a tank after flowing through a compressor in order to store a higher amount of hydrogen in a given occupied area for reducing the footprint of the storage tank.

2.3 Fuel cell Stack Unit

Fuel cell technology is similar to the previously described electrolyzers', however, the process is reversed. A fuel cell utilizes hydrogen, which is stored in tanks, and oxygen from the air and produces electricity and water. Similar to PEM electrolyzer technology, a PEM fuel cell operates at low temperatures, hence its low start-up time. Mainly, PEM fuel cells are associated with transport and stationary applications, like heavy-duty trucks and buses. [21]

A fuel cell module can supply dc loads, and it can operate in three phase connection by the use of a power inverter and a transformer in some applications as illustrated in Figure 2.4. [22], [23]

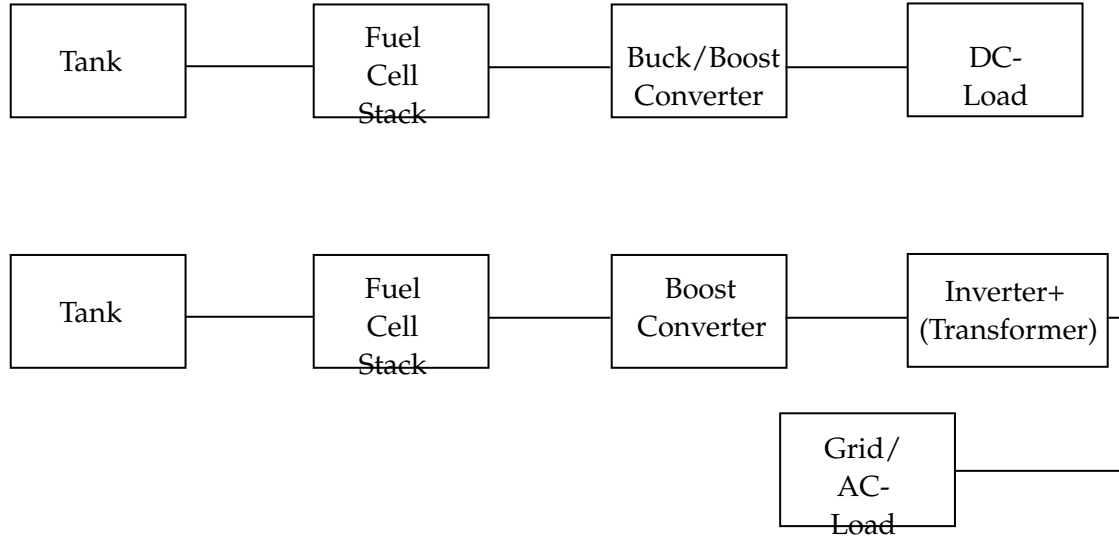


Figure 2.4: Single line diagram showing possible topologies used in fuel cell unit application related to dc- and ac connection

2.4 Load

The load to be supplied by the wind power plant is considered a town with varying load demand. The load demand is an active power.

2.5 Utility grid

The utility grid is a low-voltage distribution grid connected to the wind power plant and a town representing the variable load through two transformers and a 20 km line as illustrated in Figure 2.5.

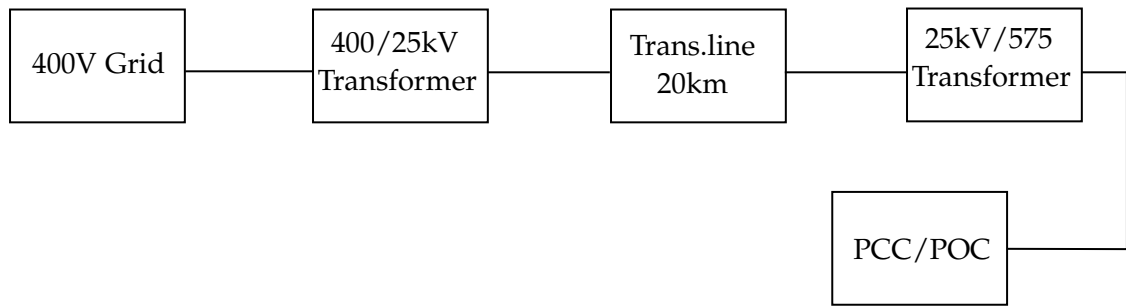


Figure 2.5: Single line diagram of the utility grid

2.6 Summary

Chapter 2 has presented the layout of the adopted system to provide an overview of the expected components and their location. Additionally, a brief description of each component has been included in this chapter.

Chapter 3

Modeling and Model Verification

This chapter presents the modeling approach of the proposed system. Additionally, the control method is also presented in this chapter.

3.1 Modelling

In this section, the components of the proposed system, which is presented in Figure 2.1 are to be modeled separately and assembled to form the total system.

3.1.1 Wind Power Plant

The type-3 wind power plant consists of an aerodynamic part, gearbox, doubly-fed induction generator, and back-to-back converter connecting the rotor of the generator to the grid as seen in Figure 2.2. The mechanical energy of the aerodynamic part is a function of wind speed and the power coefficient (C_p) of the wind turbine. The C_p is determined by the tip-speed ratio, the radius of the turbine's rotor, and the pitch angle. Equations 3.1 and 3.2 determine the mechanical power of the wind turbine and its tip-speed ratio. [20]

$$P_m = 0.5 \cdot \rho \cdot A \cdot C_p(\lambda, \beta) \cdot V^3 \quad (3.1)$$

Where A is the area swept by the wind turbine's rotor.

$$\lambda = \frac{\omega \cdot \text{Radius}}{V} \quad (3.2)$$

In order to operate the wind turbine at the maximum power point, the turbine's power coefficient (C_p) must be at its maximum, which is around 0.48. The control approach is found in many pieces of literature e.g. [20], [24] and [25]. Figure 3.1 illustrates the structure of the aerodynamic part of the wind turbine.

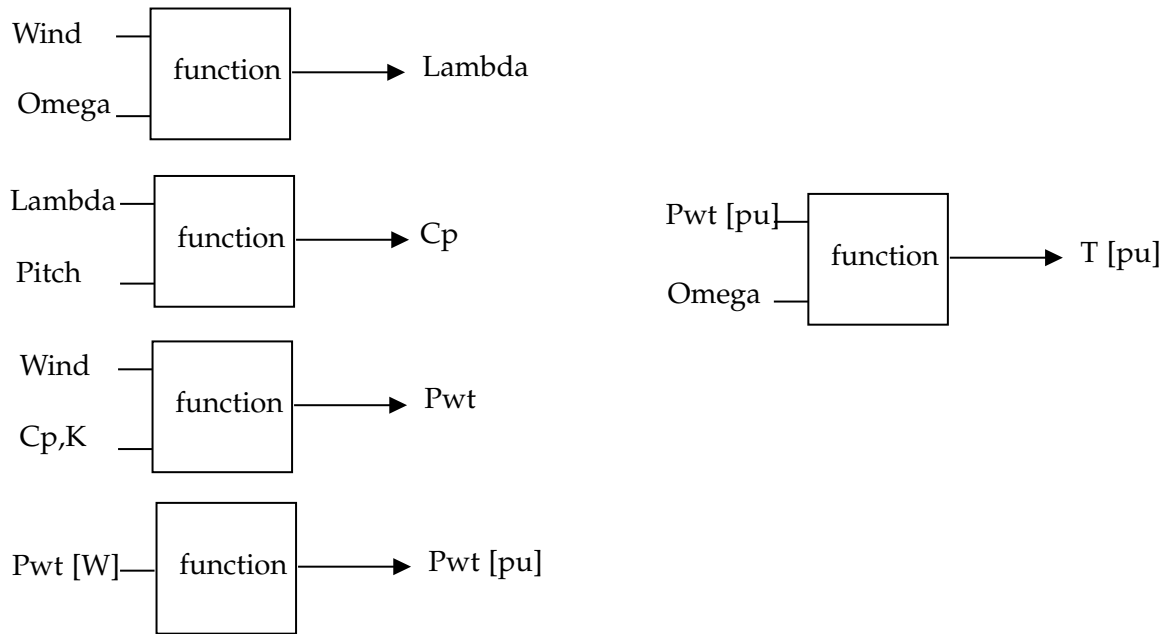


Figure 3.1: Block diagram showing the implementation of the aerodynamic part

The parameters used in the implemented wind power plant are shown in Table 3.1

Parameter	Value
Nominal power	1.5 MW
Nominal Stator voltage	575 V
Nominal Rotor voltage	1975
Nominal current	1.51 kA
DC-bus voltage	1150 Vdc
Lm	2.9 pu
Frequency	50 Hz
Inertia constant	4.32 s
Rated wind speed	11 m/s

Table 3.1: Parameters of the wind turbine

3.1.2 Electrolyzer plant

A 50 kW PEM electrolyzer unit is to be implemented, due to its advantages over an alkaline electrolyzer regarding the size footprint and power consumption. [26]

An electrical representation of a single PEM electrolyzer can be illustrated by

an equivalent circuit as shown in Figure 3.2.

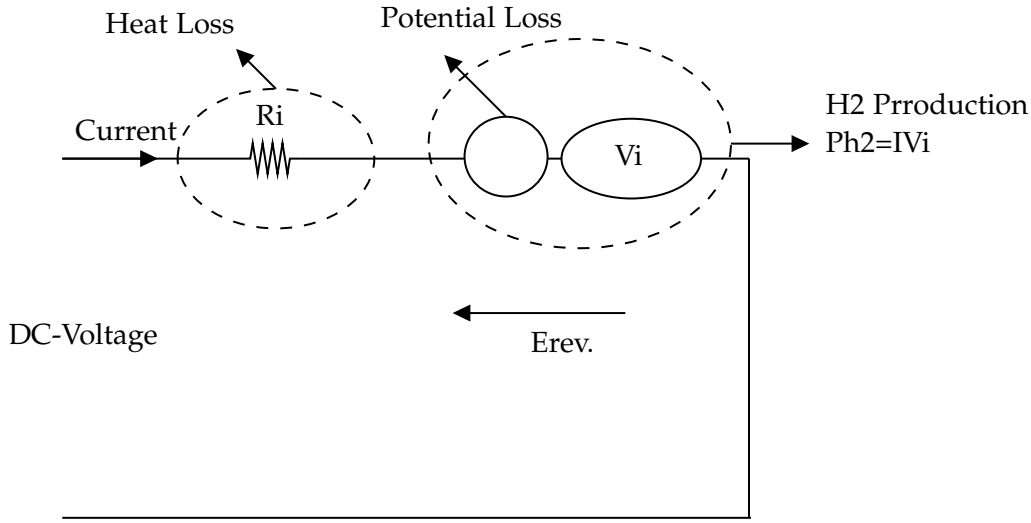


Figure 3.2: Layout of an equivalent electrical model of a PEM electrolyzer, inspired by [4]

A mathematical model of a PEM electrolyzer system is based on a set of equations from Equation 3.6 to Equation 3.8. [4], [27]

The V-I characteristic curve of a single PEM electrolyzer is given in Equation 3.3.

$$V(T, p) = e_{rev}(T, p) - e_{rev}(T, p) \cdot e^{\frac{-5I}{0.02}} + I \cdot R_i(T, p) \quad (3.3)$$

Where:

- $e_{rev}(T, p)$ is reversible potential as a function of temperature T and pressure p .
- I is the input current.
- $R_i(T, p)$ is the resistance of a PEM cell as a function of temperature and pressure.

The reversible potential $e_{rev}(T, p)$ and the resistance of the cell $R_i(T, p)$ can be determined by using Equation 3.4 and Equation 3.5, respectively.

$$e_{rev}(T, p) = e_{rev0} + \underbrace{\frac{R \cdot (273.15 + T)}{2F}}_{v_m} \cdot \ln\left(\frac{p}{p_0}\right) \quad (3.4)$$

$$R_i(T, p) = R_{i0} + k \cdot \ln\left(\frac{p}{p_0}\right) + dR_t(T - T_0) \quad (3.5)$$

Where:

- e_{rev0} is the standard reversible potential.
- R is the ideal gas constant.
- F is Faraday's constant.
- v_m is the molar volume.
- R_{i0} is the standard resistance.
- k is the curve fitting parameter.
- dR_t is the resistance coefficient.

The total voltage of a PEM electrolyzer stack for a given number of cells connected in parallel, n_p , and a given number of cells connected in series, n_s , is obtained in Equation 3.6

$$V(T, p) = I \frac{n_s}{n_p} R_i(T, p) + n_s \cdot e_{rev}(T, p) \quad (3.6)$$

For a PEM electrolyzer that consists of only cells connected in series, the total voltage equation becomes 3.7.

$$V(T, p) = n_s \cdot \left(I \cdot R_i(T, p) + e_{rev}(T, p) \right) \quad (3.7)$$

The hydrogen production rate is expressed in Equation 3.8

$$v_{H_2} = n_s \cdot \frac{v_m \cdot I}{2F} \quad (3.8)$$

In order to express the production rate in ml/min , v_{H_2} shall be multiplied by $6 \cdot 10^4$.

The produced hydrogen is stored in a hydrogen tank, which is modeled according to Equation 3.9.

$$P_b - P_{bi} = Z \cdot \frac{v_{H_2} \cdot R \cdot T}{M_{H_2} \cdot V_t} \quad (3.9)$$

Where;

- P_b and P_{bi} are the tank pressure and the initial tank pressure, respectively.
- Z is the compressibility factor, which is determined by $P \cdot V_m / R \cdot T$. item $_{H_2}$ is the molar mass of the hydrogen.
- V_t is the volume of the tank.

The wind power plant powers the PEM electrolyzer by using a step-down converter that outputs a 400 Vdc as demonstrated in Figure 3.3.

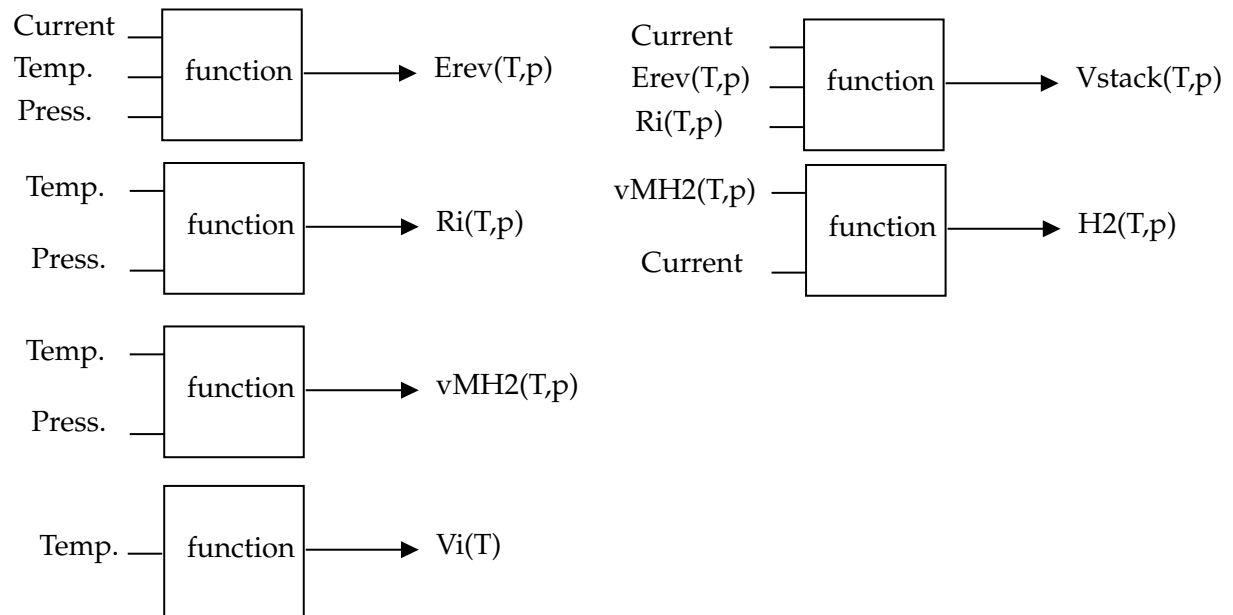


Figure 3.3: Block diagram showing the implementation of the PEM electrolyzer

3.1.3 Fuel cell model

As mentioned in Chapter 2, the PEM fuel cell structure is similar to the electrolyzer, yet the operating principle is reversed. However, as stated in the limitations of the thesis framework an equivalent dc-voltage source is used to represent the fuel cell stack. This representation is valid based on assuming that the hydrogen needed to power the fuel cell will be always available.

The PEMFC stack is connected to the PCC through a boost inverter and a designed LCL filter. The fuel cell voltage is stepped-up to 1150 V and then an inverter converts the boosted dc-voltage to ac as illustrated in Figure 3.4.

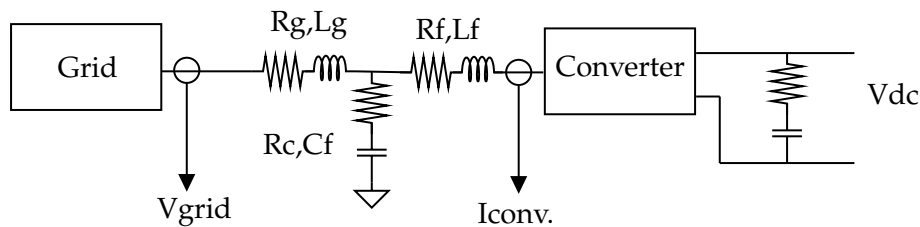


Figure 3.4: Single line diagram of a converter/ inverter

The voltage is sensed after the LCL filter, whereas the current is sensed after the converter as shown in Figure 3.4. The angle is estimated by a PLL which will be used to perform reference frame transformations for both the measured voltage and current. The current control loop is shown in Figure 4.6

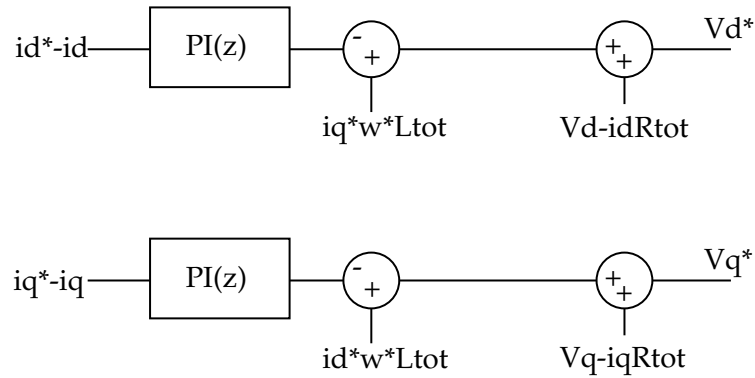


Figure 3.5: Block diagram of the current control loop

Then the reference voltage is converted back to the ABC frame which will be connected to a two-level PWM generator block that will provide the switching signals to the converter. The design procedure of the LCL filter is described in B.

3.1.4 Buck converter

This converter is implemented to step down the voltage to the operating level of the proposed PEM electrolyzer unit. The typical topology of the buck converter is illustrated in Figure 3.6.

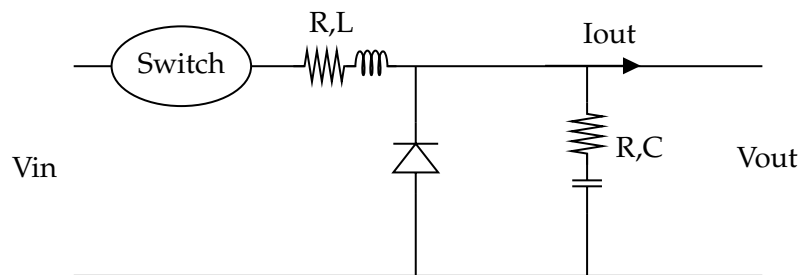


Figure 3.6: Topology of buck converter

The design parameters are demonstrated in Table 3.2. Additionally, the design procedure is described in Appendix A.

Parameter	Value
Vin	800 Vdc
Vout	400 Vdc
Rated power	50 kW
Inductor	2.9 mH
Capacitor	3.2 uC

Table 3.2: Overblik over cases.

3.2 Model Verification

In this section, the performance of the modeled systems is illustrated, where the behavior of each subsystem is analyzed individually before assembling the proposed total system which has been visualized in Figure 2.1.

Wind Power Plant

Different wind speeds have been used in order to observe the performance of the wind turbine, namely from 8 to 13, which are around the rated wind speed of the wind turbine. In this implementation, the wind turbine is operating in grid-connected mode and is not supplying any local loads. As there is no soft start-up considered in the implementation, spikes are seen during the start-up of the wind turbine as Figure 3.7 illustrates.

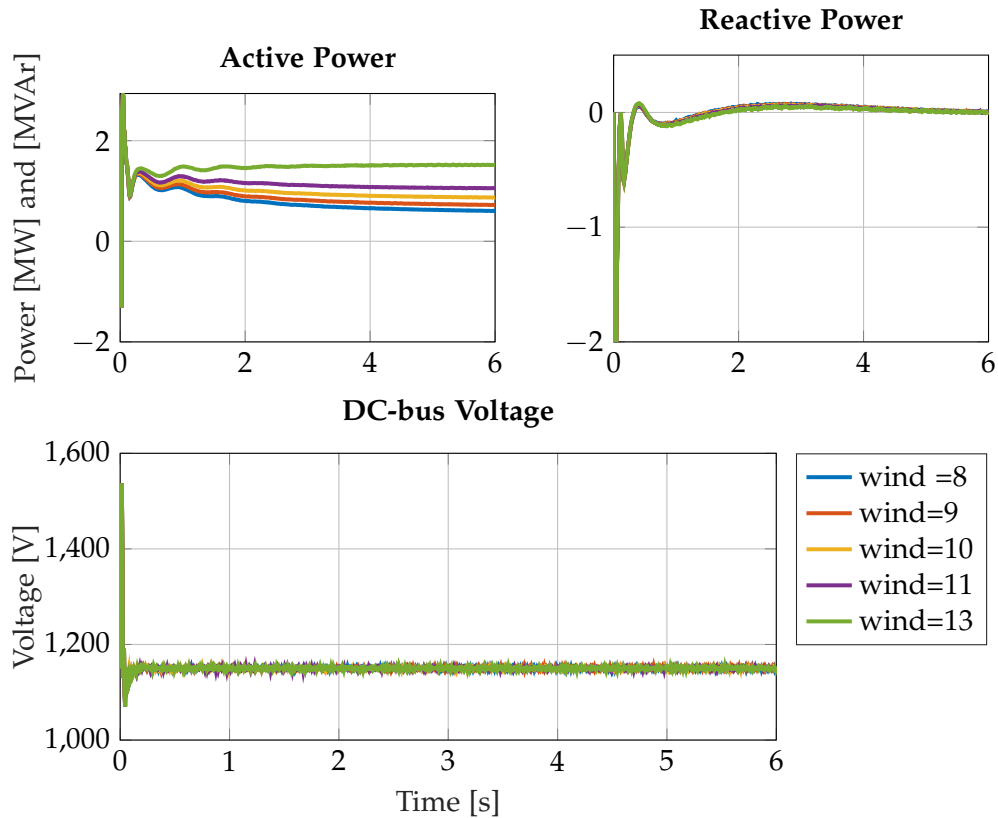


Figure 3.7: Verification of the wind power plant model

Figure 3.7 shows in the top-left of the figure fluctuation in the generated active power due to the start-up condition and the inertia of the wind turbine. However, the generated power is stabilized after around 4 seconds, corresponding to the inertia of the system. Additionally, there is reactive power exchange between the wind turbine and the grid, due to the start-up of the system. However, the reactive power becomes approximately zero after the start-up phase, due to the reactive power regulator that is implemented in the wind turbine as shown in the top-right plot in the figure. Moreover, the dc-bus voltage is kept equal to the desired value 1150 V despite the initial spike as seen in the bottom plot in Figure 3.7.

PEM Electrolyzer Model

The Electrolyzer model is connected to an ac-voltage source through a step-down converter and LCL filter. The voltage and current at the connection point to the voltage source can be seen in Figure 3.8.

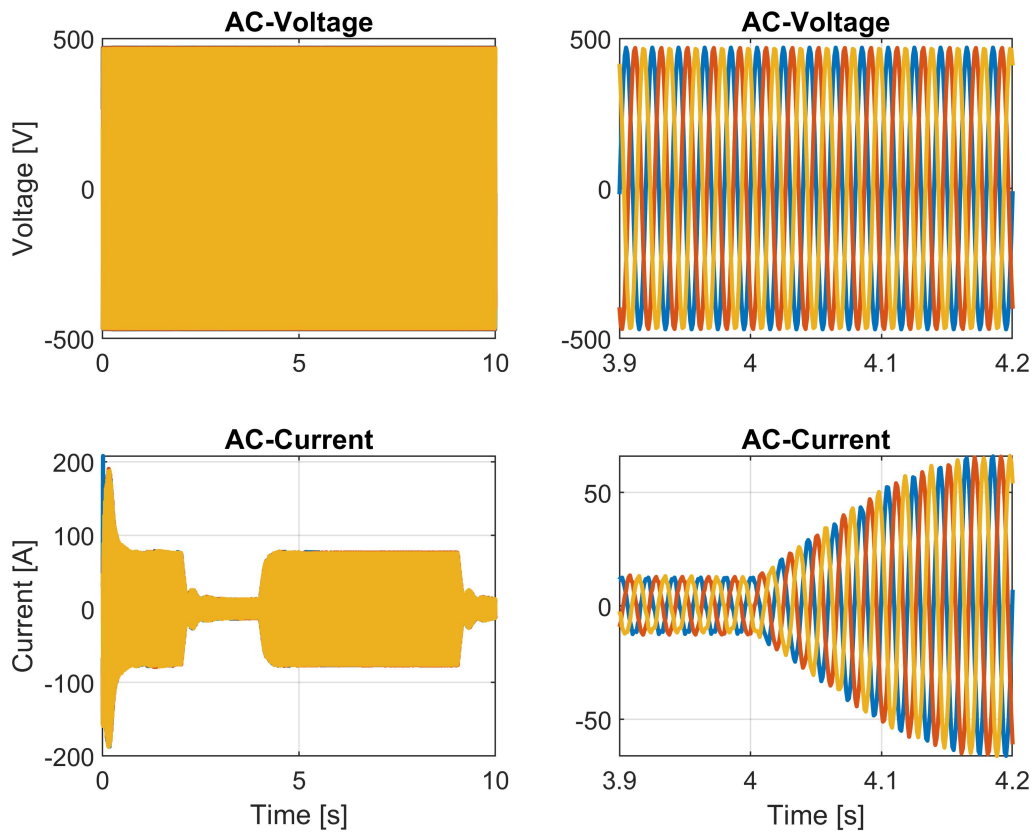


Figure 3.8: Voltage and current profiles at the converter powering the electrolyzer

Figure 3.8 shows the behavior of the voltage and the current as the electrolyzer is switched on and switched off at time equals 4 seconds and 8 seconds, respectively. The ac-current reaches the rated value, 61.5 A, as shown in the bottom-right plot in the figure.

Additionally, The active and the reactive power profiles during each switching time of the electrolyzer are illustrated in Figure 3.9.

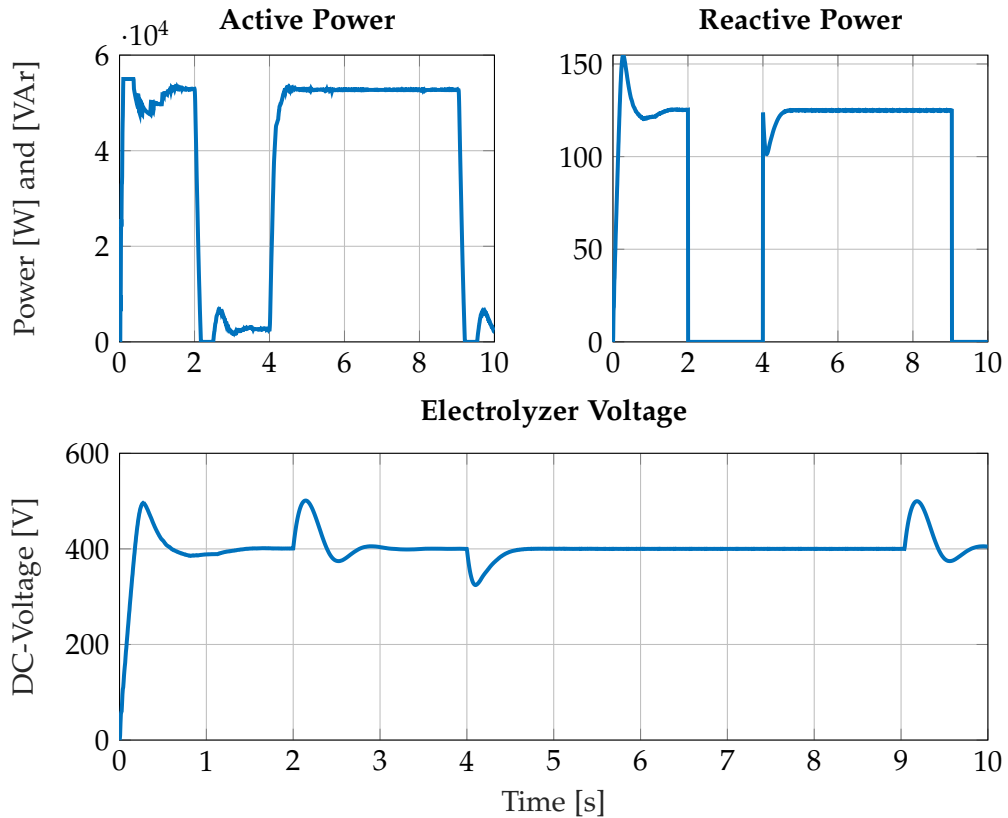


Figure 3.9: Active and reactive power supplied to the electrolyzer, and the dc- input voltage of the electrolyzer

In the top-left plot in Figure 3.9, the active power is equal to the expected power of the electrolyzer, when switching on the electrolyzer with observed perturbation due to the switch and energization of the implemented LCL filter, which is stabilized after the energization and de-energization stages are over. This is observed at time 4 seconds, where the electrolyzer is switched on during the second cycle.

The top-right plot displays an exchange in reactive power between the system and the source which is mainly due to the energization of the LCL filter. This exchange is 125 VAR corresponding to 0.0025 pu, which can be neglected.

The bottom plot in the figure illustrates the voltage profile after stepping down the voltage to the required level with over-voltage and voltage drop during connecting and disconnecting the electrolyzer, respectively. The voltage deviation is mitigated by the regulator and yields the desired voltage level.

The produced hydrogen is stored in a tank, and its flow rate during the switching of the electrolyzer are visualized in Figure 3.10

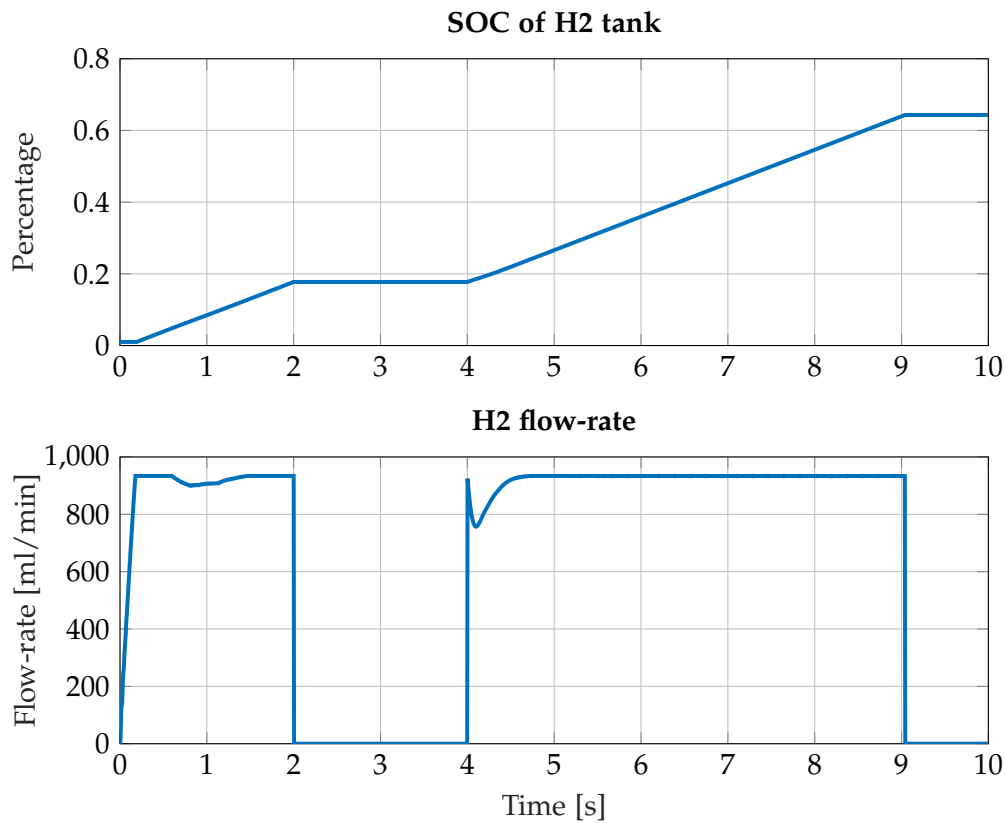


Figure 3.10: State of charge of the hydrogen tank and the produced hydrogen flow rate

The top plot in Figure 3.10 shows that the stored hydrogen is increasing during powering the electrolyzer and is kept constant when the electrolyzer is switched off as no hydrogen-consuming unit is implemented. Moreover, the estimated flow rate of the produced hydrogen is shown in the bottom plot of the figure. A fluctuation in the flow rate is observed at time 4 seconds due to the perturbation of the supplied voltage which affects the current used by the electrolyzer as defined in Equation 3.8. However, the flow rate of the produced hydrogen becomes stable after stabilizing the current.

Fuel Cell Model

To verify the behavior of the fuel cell model. An equivalent dc-voltage source is connected to the grid through an inverter and LCL filter as stated previously. The implemented model injects current into the grid when switching on and during switching off the system the current becomes zero as Figure 3.11 shows.

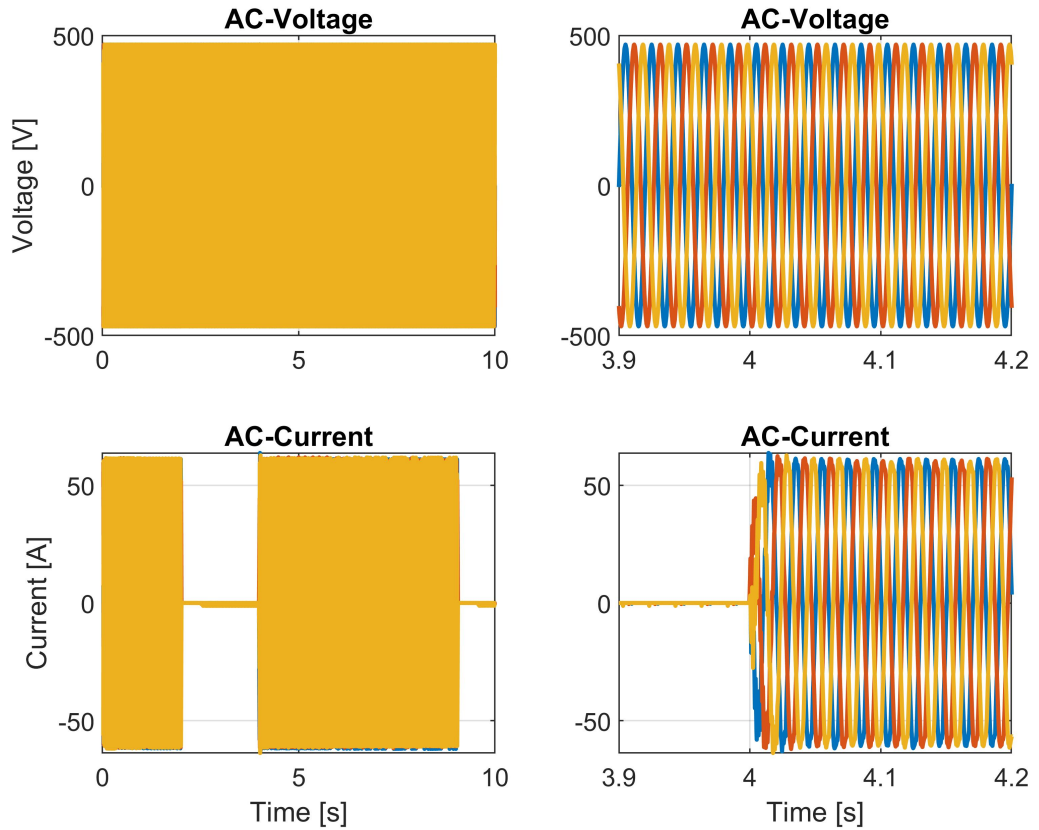


Figure 3.11: Voltage and current profiles of the fuel cell stack during performed switchings

Figure 3.11 illustrates the voltage and current profiles of the implemented system during connecting and disconnecting the system. In the bottom-right plot, the current injected current is shown as the system is switched on at time 4 seconds. The current reaches the rated value after the switching instant.

The injected power is illustrated in Figure 3.12 as the system is disconnected and reconnected at time 2 seconds and 4 seconds, respectively.

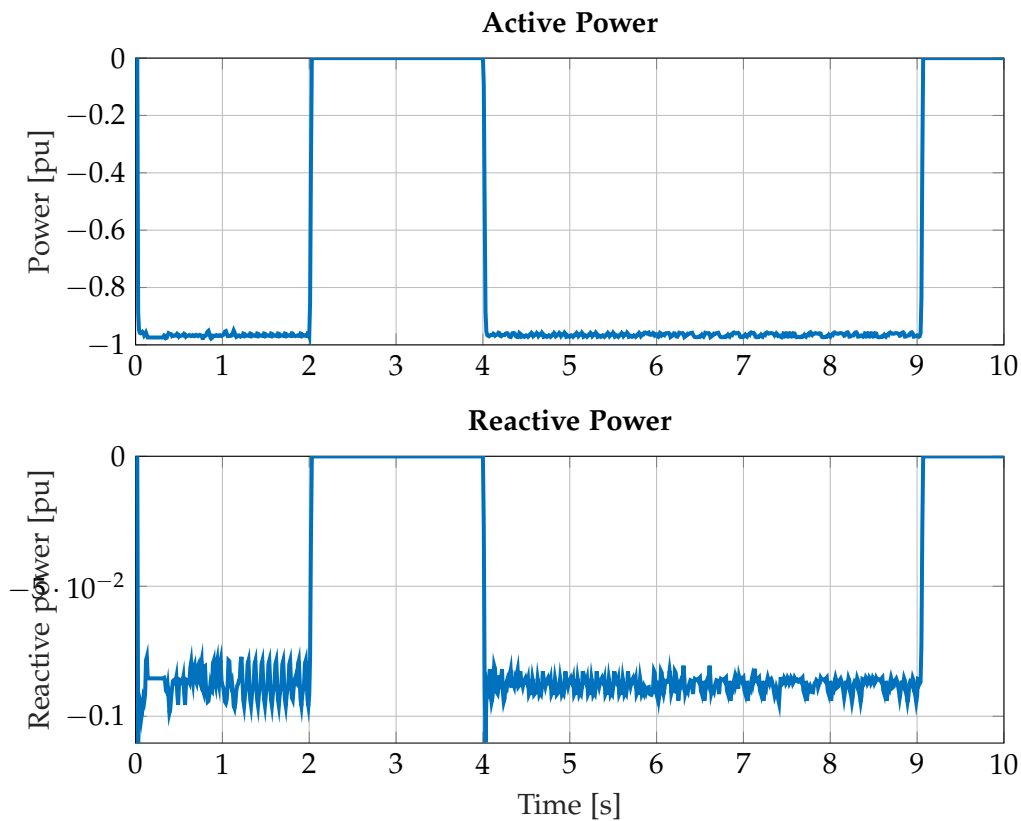


Figure 3.12: Active and reactive power profiles exchanged by the fuel cell system

The top plot in Figure 3.12 shows the active power injected into the grid by the system, which is around 1 pu, which is displayed as negative to indicate that the power flows towards the grid. However, the opposite power flow direction is observed regarding the reactive power, due to the energization of the LCL filter components.

3.3 Summary

Chapter 3 has provided the reader with the used modeling approach for each component in the proposed system. Moreover, the performance of the modeled components has been verified and thereby the proposed system can be assembled to conduct sensitivity analysis in Chapter 4.

Chapter 4

Assessment Studies

This chapter includes an assessment study of the proposed system, where the control algorithm is implemented to assess the grid support functionality of the system when the grid connection undergoes disturbances.

4.1 Case study

The proposed system operated in a grid-connected mode, where a programable fault occurs at time 1 second and is cleared at time 4 seconds. During the fault, the wind power plant and the power-to-X system are required to supply the load or a determined amount of the load demand until the fault is cleared and the grid connection is re-established.

The proposed control algorithm implemented to improve frequency support is based on power balancing power production and load demand without derating the wind power plant.

The control algorithm checks the status of the grid connection and based on the status it runs a set of checks in order to determine the amount of load to be supplied based on the available power from the wind power plant. The capacity of the power-to-X units provides the margin according to which the determination of the allowable load is performed as illustrated in Figure 4.1.

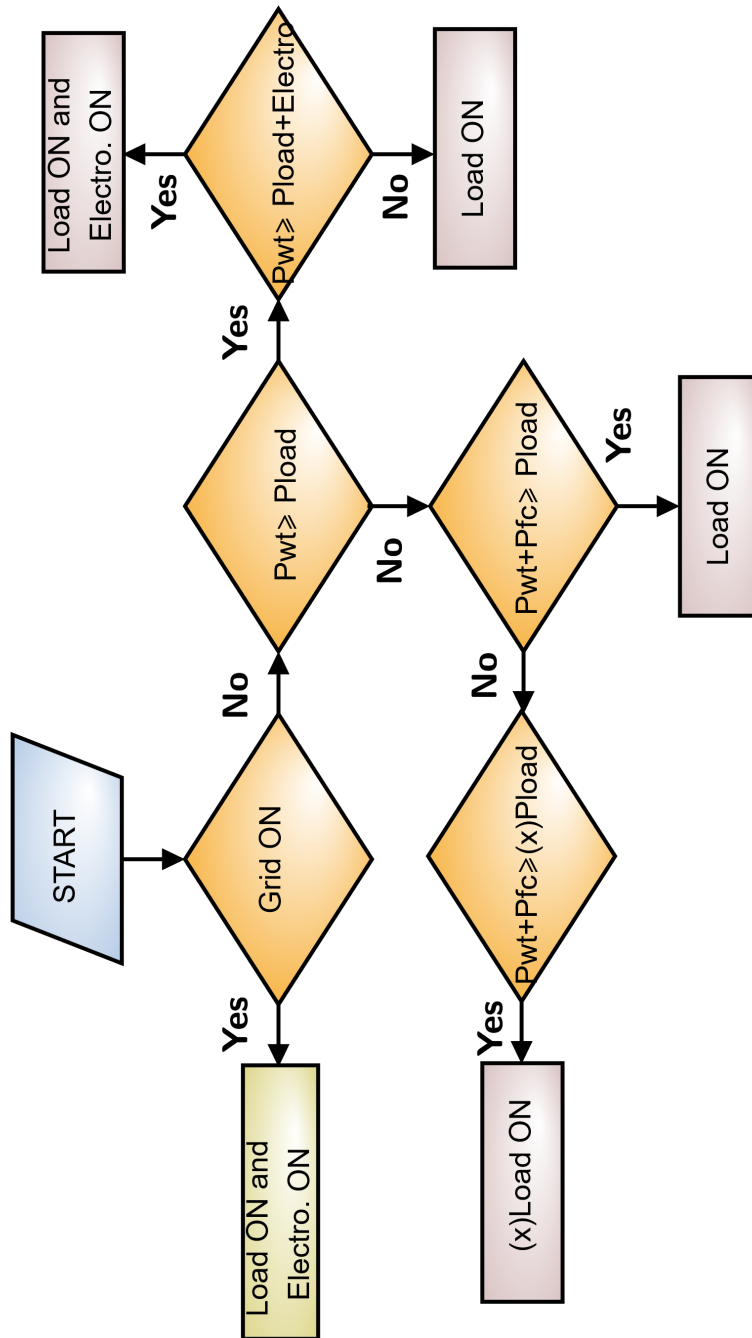


Figure 4.1: Flow chart of the developed control algorithm

In the control algorithm shown in Figure 4.1, X denotes the amount of the existing load demand that can be supplied by the proposed system, which corresponds

to the estimated power by the wind turbine at the instant of the fault \pm electrolyzer and fuel cell stack.

In this case study, the wind turbine operates below its rated capacity, when the fault occurs. The voltage and current profiles are shown in Figure 4.2 at the point connecting, the wind power plant, electrolyzer, fuel cell stack, and load, is referred to as PCC in this case study.

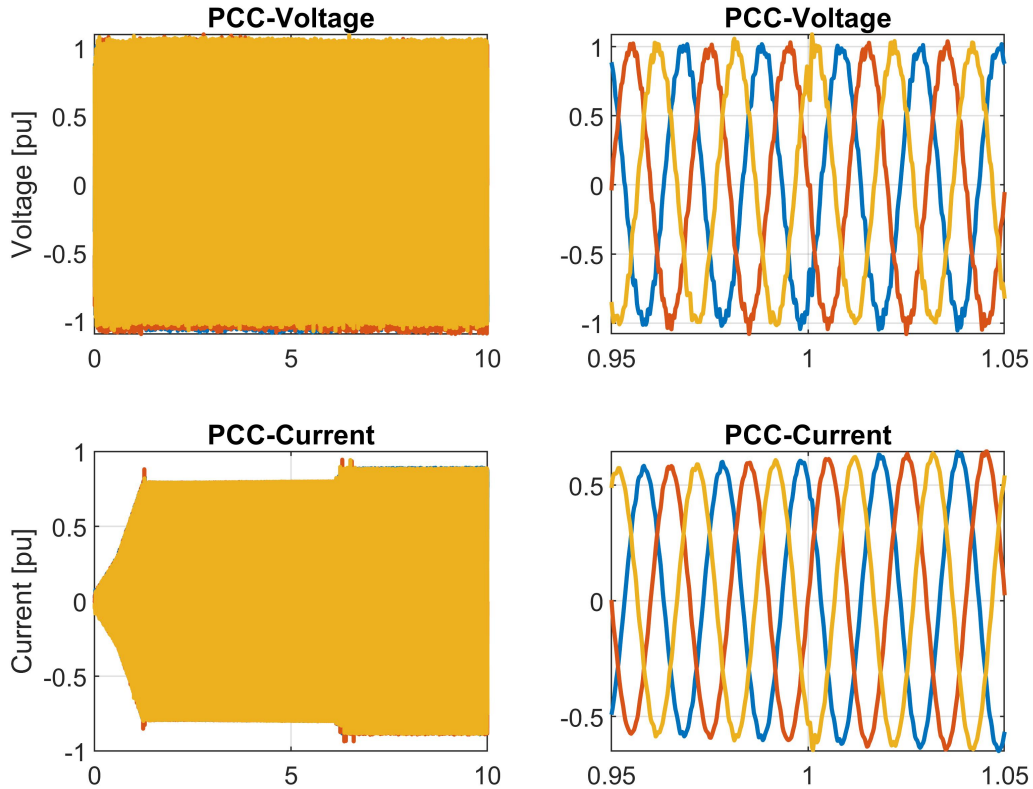


Figure 4.2: Voltage and current profiles measured at the point of connection

Figure 4.2 shows that the voltage profile is kept within the desired level around 1 pu with voltage drop occurring at time 1 second. The voltage drop is mitigated by the control algorithm as can be seen in the following figures.

At the instant of the fault, the implemented control algorithm disconnects the electrolyzer, since the estimated wind power plant power is under the rated capacity and the operating condition satisfies the condition $P_{wt} + P_{fc} \geq X \cdot P_{Load}$ as illustrated in the flow chart 4.1. Here, X is determined to be 0.8 pu of the total load demand with a safety margin of ± 100 kW corresponding to connecting and disconnecting the electrolyzer unit and the fuel cell stack with a time duration

equivalent to the wind power plant inertia.

The power profile of the system components is illustrated in Figure 4.3

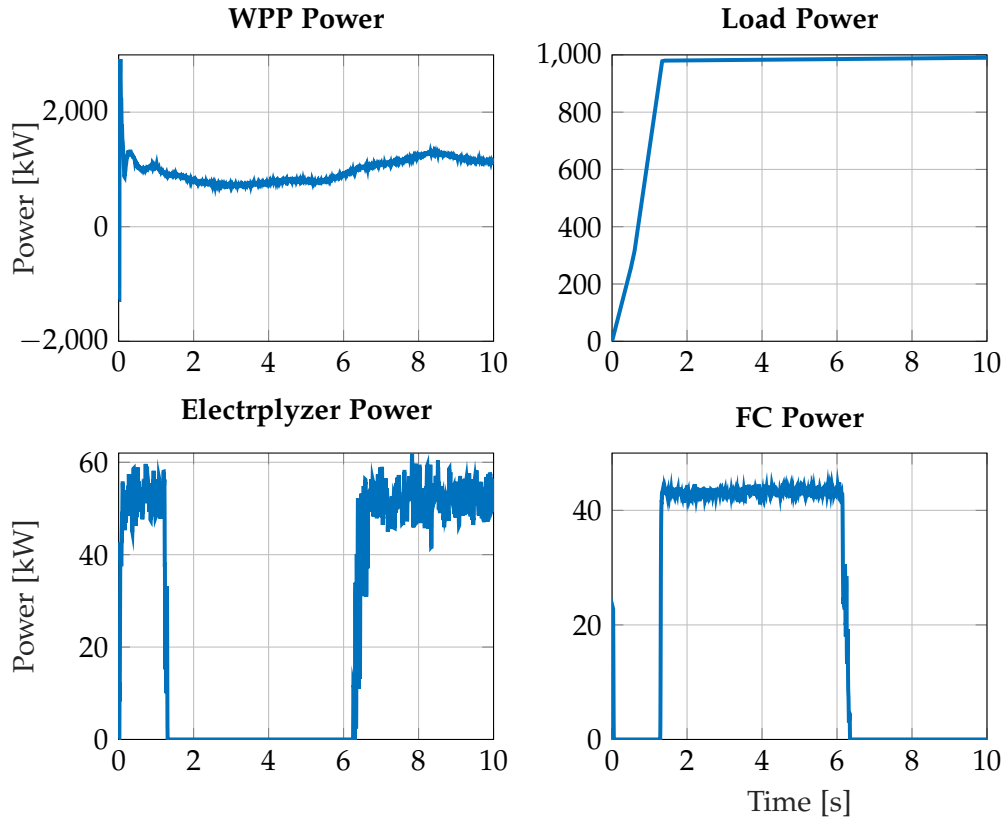


Figure 4.3: Power profile of the power generating and consuming units

Figure 4.3 shows the power profile generated by the wind power plant, where at time around 1.3 seconds the operating condition violates $P_{wt} \geq X \cdot P_{Load} + P_{electro}$, leading to disconnecting the electrolyzer, directly connecting the fuel cell system and setting a maximum load corresponding to $P_{wt} + P_{fc} \geq X \cdot P_{Load}$.

Moreover, the time instants at which the switchings are occurring for both the electrolyzer system and the fuel cell system are shown in 4.3.

The voltage and current profiles of the electrolyzer system are visualized during and after clearing the fault in Figure 4.4

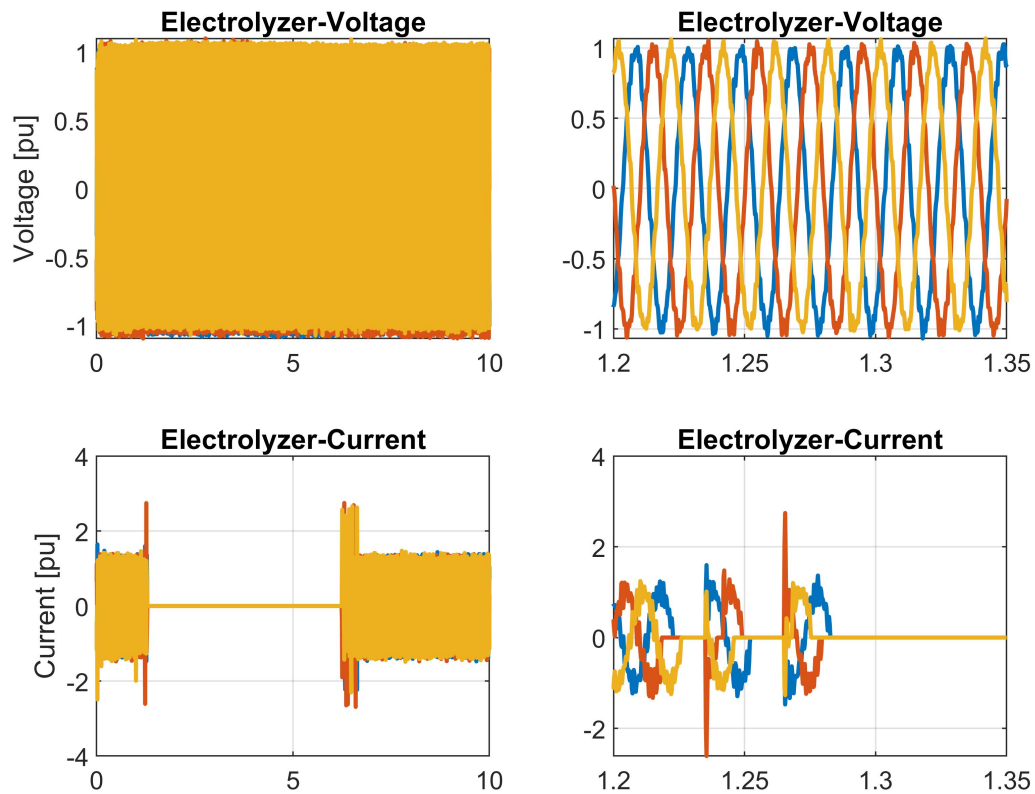


Figure 4.4: Voltage and current behavior measured at the converter powering the electrolyzer

In Figure 4.4, the voltage profile shows a satisfying voltage level that does not affect the voltage at PCC and the current is zero as the unit is switched off at the instant of violating the condition set in the control algorithm. It is also observed that even though the grid connection is restored at time 4 seconds, the electrolyzer is not allowed to be connected as the control algorithm prioritizes supplying the loads by the wind power plant until time 3 seconds to check the stabilization of the grid connection.

In contrast to the switching process of the electrolyzer system, the fuel cell stack is connected at the instant the electrolyzer violates the condition, as illustrated in Figure 4.5.

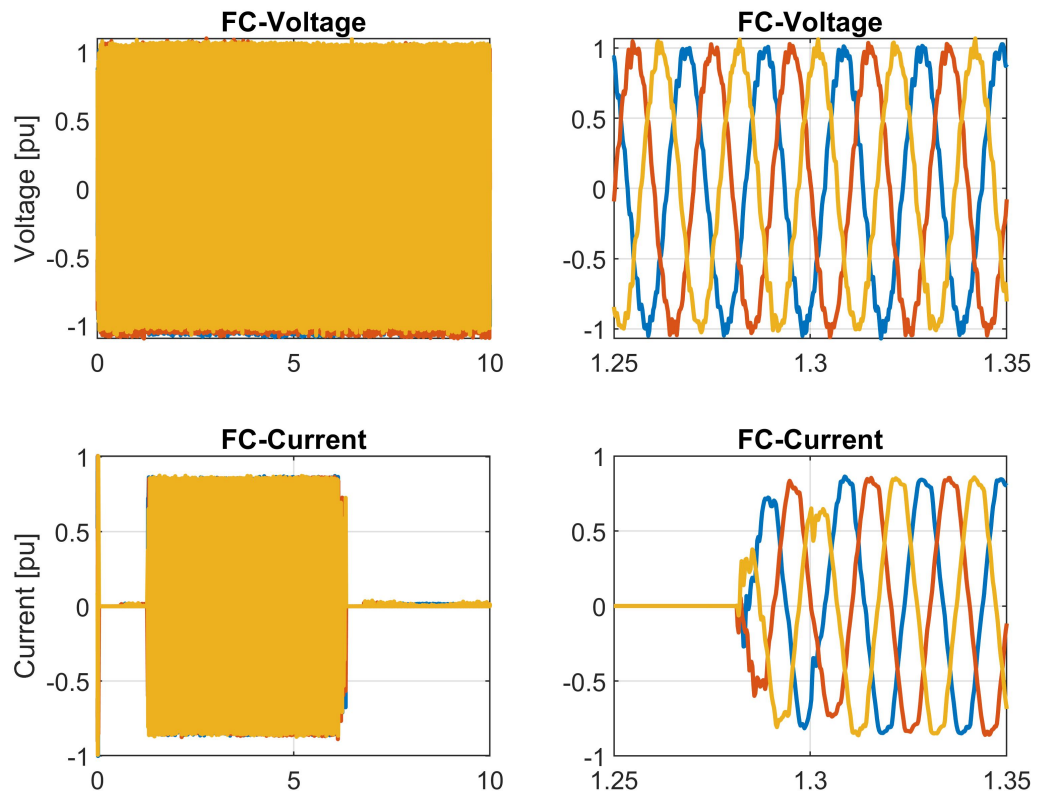


Figure 4.5: Voltage and current profiles measured at the inverter supplied by the fuel cell stack

Figure 4.5 shows both the voltage and current profiles of the fuel cell system as it is switched on around time 1.3 seconds. Similar to the behavior of the electrolyzer, the control algorithm delays the disconnection of the fuel cell system after the restoration of the grid connection as shown in the bottom left plot in Figure 4.5.

Lastly, the frequency profile of the proposed system satisfies the frequency grid support criterion as the frequency is kept around 50Hz with a drop occurring at the instant of losing the grid connection at time 1 second. The drop corresponds to 0.0032 pu.

Moreover, a spike in the frequency is observed when the fault is cleared corresponding to 0.0033 pu. After restoring the grid connection, it is observed that the frequency profile is maintained around the desired value.

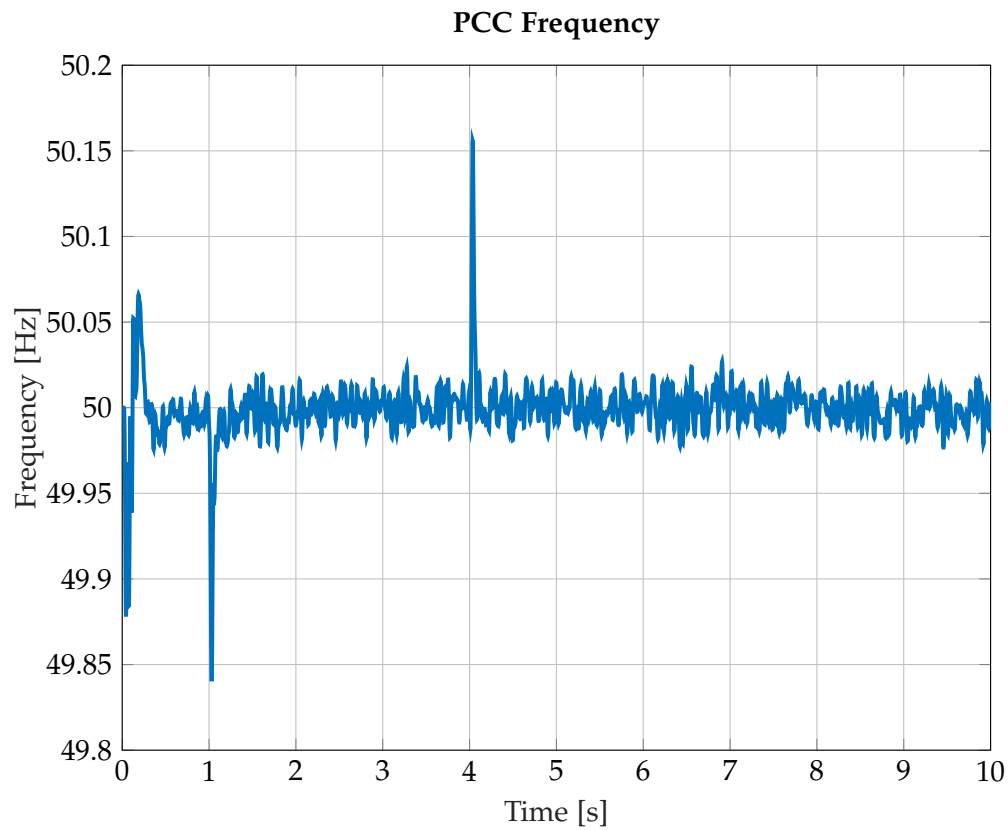


Figure 4.6: Frequency profile during the simulation

4.2 Summary

Chapter 4 has presented a sensitivity analysis of incorporating the electrolyzer and fuel cell to aid a wind power plant in providing a power system balance by the use of a developed control algorithm. This performance of the system has shown satisfactory results complying with the adopted grid code.

Chapter 5

Conclusion and Future work

This chapter provides a conclusion of the report that summarises the conducted work during this project work with a focus on addressing the introduced objectives presented in Chapter 1. Moreover, the chapter includes potential future work and recommendations that can be considered to touch upon for further development in this area.

5.1 Conclusion

Chapter 1 has provided the reader with an introduction to the increasing tendency to integrate wind power plants into the utility grid worldwide and especially in Denmark with its 2030- and 2050 plans, respectively. However, due to the challenges associated with this technology, a potential solution approach that has been considered is the incorporation of power-to-X technology, particularly power-to-H₂. This chapter has also shown that this technology can be utilized as power storage by the use of an electrolyzer unit in case of excess wind power production. The stored hydrogen could be used in the transport sector or grid support application by the use of fuel cell technology.

A state-of-the-art has introduced the potential approaches related to incorporating the power-to-X technology to overcome the inherent power fluctuation challenge of wind power plants in order to provide improved frequency stability.

Chapter 2 has introduced a general description of the proposed system and its components. The wind power plant has been described and a general system layout of a type-3 wind power plant has been chosen based on which the system implementation would be performed.

Additionally, this chapter has provided a description of the water electrolysis process and the electrolyzer unit, which has been chosen to be implemented in the system to produce hydrogen. Moreover, The operating principle of a fuel cell stack unit and its main applications have also been described in this chapter.

Chapter 2 has also included a description of the load and the utility grid to which the total system is connected.

The modeling approach of the proposed system described in chapter 2 has been introduced in Chapter 3, where each component of the system has been implemented in the Matlab/Simulink platform in order to conduct assessment studies for investigating the performance of the system.

Firstly, the modeling approach of the wind power plant has been introduced in the chapter. Secondly, the chapter has presented the modeling approach of the electrolyzer unit and its implementation in the Matlab/Simulink platform. Thirdly, the chapter has stated that the fuel cell unit is modeled as an equivalent dc-voltage source assuming that there would always be sufficient hydrogen to operate the fuel cell unit. Fourthly, Chapter 3 has included the modeling and control method for power converter units that have been used to connect the previously mentioned components.

Lastly, Chapter 3 is concluded with model verification where the behavior of the modeled components has been verified before investigating the performance of the proposed system.

Chapter 4 has presented a case study in order to analyze the performance of the total system where the grid connection is compromised and the electrolyzer together with the fuel cell units has to contribute to grid frequency support and aiding the wind power plant in supplying the load. Chapter 4 has also introduced the developed control algorithm based on which the role of the electrolyzer and the fuel cell would be given according to the power produced by the wind power plant with respect to the demanded load.

The Case study presented in this chapter has shown satisfactory results as the frequency at the point of connection has been kept within the required range without compromising the voltage profile. This result has been obtained by connecting or disconnecting the electrolyzer in order to add or remove its load and by incorporating the fuel cell unit to provide electric power if the load is higher than the estimated power from the wind power plant.

Based on the results of the conducted case study, the problem formulation has been answered and the objectives that have been presented in chapter 1 have been addressed.

5.2 Future work and Recommendations

As the scope of the project has been narrowed due to time limitations, potential further work can be conducted in this field, the following points can potentially contribute to a more detailed assessment of the performance of the proposed system.

- Investigating the impact of utilizing a larger electrolyzer unit capacity, that might be consisting of small electrolyzer units like Siemens's module which is a PEM type and has rated stack power in the range of MW (https://www.heattofuel.eu/wp-content/uploads/2021/03/6_lona-Dickschas.pdf).
- Investigating the impact of implementing an actual model of the fuel cell stack in order to incorporate the time delay for starting up the unit.
- Assess the performance of the system when implementing multiple wind turbines and different loading locations.
- Comparing the performance of the system when controlled by a different control method for example power factor control.
- Investigate the feasibility of operating the proposed system in accordance with the market prices.

Bibliography

- [1] International Energy Agency (IEA). Global energy review 2021. <https://www.iea.org/reports/global-energy-review-2021/renewables>, last seen: 13.10.2022, 2021.
- [2] International Energy Agency (IEA). Electricity generation by source, denmark 1990-2020. <https://www.iea.org/fuels-and-technologies/electricity>, 2020.
- [3] Xuetao Xing et al. Modeling and operation of the power-to-gas system for renewables integration: A review, csee journal of power and energy systems. <https://ieeexplore.ieee.org/stamp/stamp.jsp?tp=&arnumber=8386629>, Last seen on 13-10-2022.
- [4] Stefan Krauter Marius C. Möller. Hybrid energy system model in matlab/simulink based on solar energy, lithium-ion battery and hydrogen. <https://www.mdpi.com/1996-1073/15/6/2201/htm>, Last seen on 13-10-2022.
- [5] Mahmoud Badreldien, Rana Usama, Amged El-Wakeel, and Almoataz Abdelaziz. Modeling, analysis, and control of doubly fed induction generators for wind turbines, 05 2014.
- [6] Danish energy agency. Data: Oversight over energisektoren. <https://ens.dk/service/statistik-data-noegletal-og-kort/data-oversigt-over-energisektoren>, 2021.
- [7] Bikash Kumar Sahu. Wind energy developments and policies in china: A short review, renewable and sustainable energy reviews, volume 81, part 1, 2018.
- [8] E. Joshua and R. Sthuthi. *Wind Power Technology*. PHI LEARNING PVT. LTD., 3. ed. edition, 2019.
- [9] VENKATA YARAMAS and BIN WU. *MODEL PREDICTIVE CONTROL OF WIND ENERGY CONVERSION SYSTEMS*. Number ISBN: 978-1-118-98858-9 in 3rd edition. Hoboken, NJ: John Wiley & Sons, 2017.

- [10] EnergiNet. Regulations for grid connection. <https://en.energinet.dk/Electricity/Rules-and-Regulations/Regulations-for-grid-connection>, 2016.
- [11] G. Lalor, A. Mullane, and M. O'Malley. Frequency control and wind turbine technologies. *IEEE Transactions on Power Systems*, 20(4):1905–1913, 2005.
- [12] Germán Claudio Tarnowski. *Coordinated Frequency Control of Wind Turbines in Power Systems with High Wind Power Penetration*. PhD thesis, 2012.
- [13] Barry G. Rawn, Peter W. Lehn, and Manfredi Maggiore. Control methodology to mitigate the grid impact of wind turbines. *IEEE Transactions on Energy Conversion*, 22(2):431–438, 2007.
- [14] Thomas Ackermann. *Wind Power in Power Systems*. Number 978-0-470-97416-2 in 2nd Ed. John Wiley & Sons Ltd, 2005.
- [15] Munendra Singh, Shailendra, Saurabh Chanana, and Dogga Raveendhra. Operation and control of a hybrid wind-diesel-battery energy system connected to micro-grid. In *2013 International Conference on Control, Automation, Robotics and Embedded Systems (CARE)*, pages 1–6, 2013.
- [16] A. Hasib Chowdhury and Md. Asaduz-Zaman. Load frequency control of multi-microgrid using energy storage system. In *8th International Conference on Electrical and Computer Engineering*, pages 548–551, 2014.
- [17] Giulio Buffo et al. Chapter 15 - power-to-x and power-to-power routes. Academic Press <https://doi.org/10.1016/B978-0-12-814853-2.00015-1>, 2019.
- [18] Danish Energy Agency (DEA). Power-to-x. <https://ens.dk/ansvarsomraader/power-x-og-groen-brint>, Last seen on 13-10-2022.
- [19] Energinet. Rule and regulations. <https://en.energinet.dk/Electricity/Rules-and-Regulations/Regulations-for-grid-connection>, Last seen on 13-10-2022.
- [20] Gonzalo Abad and Grzegorz Iwanski. *Wind Power in Power Systems*. Number 9781118755525. John Wiley & Sons, Ltd, 2014.
- [21] Frank de Bruijn. The current status of fuel cell technology for mobile and stationary applications. <https://pubs.rsc.org/en/content/articlehtml/2005/gc/b415317k>, Last seen on 13-10-2022.
- [22] Nan Zhao Renqi Guo, Quan Li. An overview of grid-connected fuel cell system for grid support, energy reports, volume 8, supplement 10. <https://www.sciencedirect.com/science/article/pii/S2352484722010575>, Last seen on 13-10-2022.

- [23] Nan Zhao Renqi Guo, Quan Li. Design considerations for dc-dc converters in fuel cell systems. <https://www.google.com/url?sa=t&rct=j&q=&esrc=s&source=web&cd=&cad=rja&uact=8&ved=2ahUKEwja5fjh7d76AhXLQPEDHVZ5DccQFnoECBYQAQ&url=http%3A%2F%2Foaktrust.library.tamu.edu%2Fbitstream%2Fhandle%2F1969.1%2FETD-TAMU-1106%2FPALMA-FANJUL-DISSERTATION.pdf%3Fsequence%3D1&usg=A0vVaw0I4NCWJsp0APTcMXk0kIz8>, Last seen on 13-10-2022.
- [24] Lihui Yang, Zhao Xu, Jacob Ostergaard, Zhao Yang Dong, and Kit Po Wong. Advanced control strategy of dfig wind turbines for power system fault ride through. *IEEE Transactions on Power Systems*, 27(2):713–722, 2012.
- [25] Miguel Rodriguez Gonzalo Abad, Jesus Lopez. *Doubly Fed Induction Machine: Modeling and Control for Wind Energy Generation*. Number 978-0-470-76865-5. John Wiley & Sons, Ltd, 2011.
- [26] Caisheng Wang. Modeling and control of hybrid wind/photovoltaic/fuel cell distributed generation systems. <https://scholarworks.montana.edu/xmlui/handle/1/2497>, Last seen on 13-10-2022.
- [27] Mohamed Albarghot and Luc Rolland. Matlab/simulink modelling and experimental results of a pem electrolyzer powered by a solar panel. In *2016 IEEE Electrical Power and Energy Conference (EPEC)*, pages 1–6, 2016.

Appendix A

Appendix A

10/14/22 8:49 AM D:\MastersThesis\Buck design Elect... 1 of 1

```
%buck converter design

%clear; clc;
Ts=5e-5; % Sampling time
fsw_buck=20e3; % Switching frequency
Po_elect=55e3; % Assumed power of electrolyzer
Vs_buck=1100; % Assumed input voltage after rectification
Vo_buck=400; % Desired output voltage
Io_buck=Po_elect./Vo_buck; % Estimated output current
D_buck=Vo_buck./Vs_buck; % Duty-cycle
dVo_buck = 0.05.* Vo_buck; % Voltage deviation/ripple
R_buck=Vo_buck./Io_buck; % Estimated output resistor
dIL_buck=0.05.*Io_buck; % Current ripple
Lmin1_buck=(1-D_buck).*R_buck/(2*fsw_buck); % Current control modulation check
Lmin2_buck=(Vs_buck-Vo_buck).*(D_buck./(dIL_buck.*fsw_buck)); % dIL check
L_buck=max([Lmin1_buck,Lmin2_buck])*2; % Inductor determination
Cmin_buck=(1-D_buck)./(8.*L_buck.*(dVo_buck/Vo_buck).*fsw_buck.^2); % Min. capacitor
C_buck=max(Cmin_buck)*3; % Capacitor determination
D_buck_vary=[0:1e-3:1]; % Assumption for plotting figures
Vo_buck=Vs_buck*D_buck_vary; % Assumption for plotting figures

figure;
subplot(2,1,1)
plot(D_buck_vary,Vo_buck.*(1-D_buck_vary)/(L_buck*fsw_buck));
hold on;
plot(D_buck_vary,ones(1,length(D_buck_vary))*dIL_buck,'--');
xlabel('duty cycle'); ylabel('d I_L [A]'); legend('d IL buck','0.2*IL')
subplot(2,1,2)
plot(D_buck_vary,Vo_buck.*(1-D_buck_vary)./(8*L_buck.*C_buck.*fsw_buck.^2));
hold on;
plot(D_buck_vary,ones(1,length(D_buck_vary))*dVo_buck,'--');
ylabel('d Vo [V]'); xlabel('duty cycle'); legend('d Vo','0.1*Vo')
hold off
```

10/14/22 8:52 AM D...\Boost design FuelCell dc level.m 1 of 1

```

% boost converter design
%clear; clc;

fsw_boost=20e3;
Vs_boost=625;
Is_boost=50e3/625;
Ps_boost=Vs_boost.*Is_boost;
Vo_boost=1150;
D_boost=1-(Vs_boost./Vo_boost);
dVo_boost=0.1.*Vo_boost;
Po_boost=Ps_boost;
R_boost=Vo_boost.^2./Po_boost;
IL_boost=Vo_boost./((1-D_boost).*R_boost);
dIL_boost=0.2*IL_boost;
Lmin1_boost=D_boost.*(1-D_boost).^2.*R_boost./(2*fsw_boost);
Lmin2_boost=Vs_boost.*D_boost./(dIL_boost.*fsw_boost);
L_boost=max([Lmin1_boost,Lmin2_boost])*2;
C_min_boost=Vo_boost.*D_boost./(R_boost.*dVo_boost.*fsw_boost);
C_boost=max(C_min_boost)*2;
D_vary_boost=0:1e-3:1;
Vs_boost=(1-D_vary_boost).*Vo_boost;
figure;
subplot(2,1,1)
plot(D_vary_boost,Vs_boost.*D_vary_boost./(L_boost*fsw_boost));
hold on;
plot(D_vary_boost,ones(1,length(D_vary_boost))*dIL_boost,'--');
xlabel('duty cycle'); ylabel('d IL'); legend('d IL','0.2*IL')
subplot(2,1,2)
Ps_boost=Vs_boost.*40; R_boost=Vo_boost.^2./Ps_boost;
plot(D_vary_boost,(D_vary_boost.*Vo_boost./(R_boost.*C_boost.*fsw_boost)));
hold on;
plot(D_vary_boost,ones(1,length(D_vary_boost))*dVo_boost,'--');
xlabel('duty cycle'); ylabel('d Vo [V]'); legend('d Vo','0.1*Vo')

```

10/14/22 8:43 AM C:\Users\BUSHR...\Filter design LCL.m 1 of 1

```
% LCL filter design & Current regulators coefficients
%clear
%clc
Prated=50e3;
vg=575*sqrt(2); %line-line
ig=Prated/3/vg;
i_sw=0.003*ig;
v_sw=0.9*vg;
vL=20*vg;
rfilter=2e-3;
f=50;
fsw=10e3;
fres=fsw/10;
Cmax=0.05*Prated/3/(vg^2*2*pi*f); %Farad
C=Cmax*0.95;
Lmin=abs(1/((2*pi*fsw)*(i_sw/v_sw)*(1-(2*pi*fsw)^2/(2*pi*fres)^2))); %Henry
Lmax=0.2*vg/(2*pi*f*ig); %Henry
L1=Lmax/2;%(Lmax+Lmin)/2;
L2=Lmax/2;%(Lmax+Lmin)/2;
Lp=L1*L2/(L1+L2);
wres=1/sqrt(C*Lp);
```

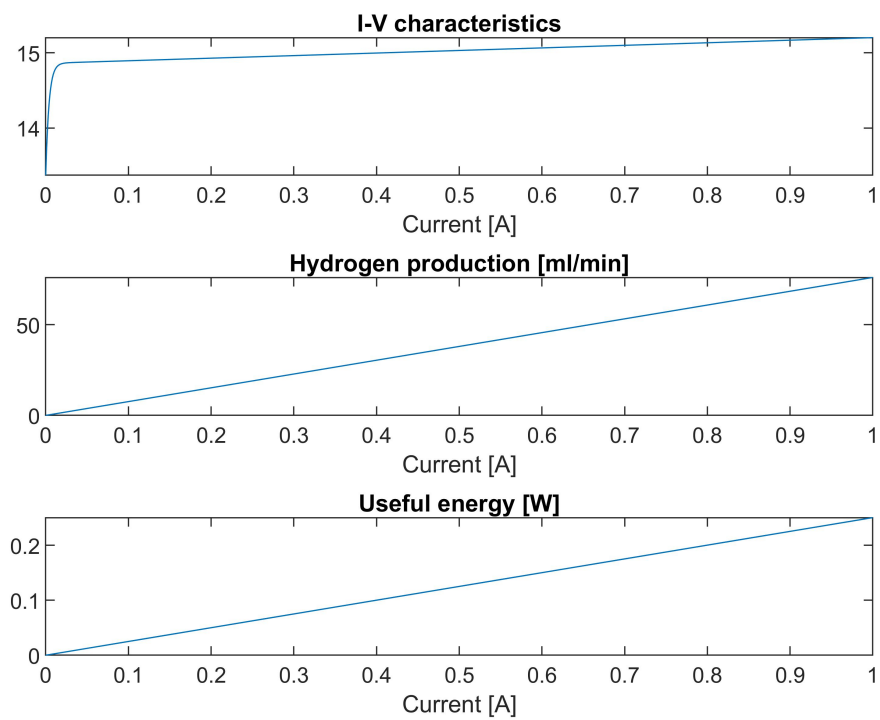


Figure A.1: VI-characteristics of a single PEM cell

Appendix B

Appendix B

Additional Case study A

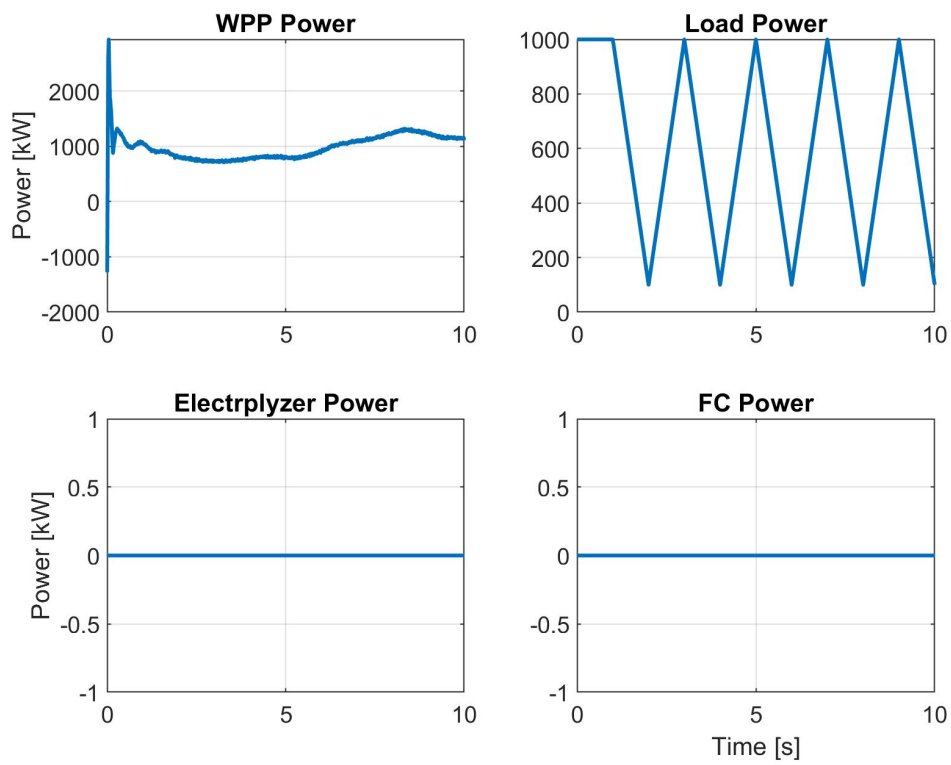


Figure B.1: Power profiles

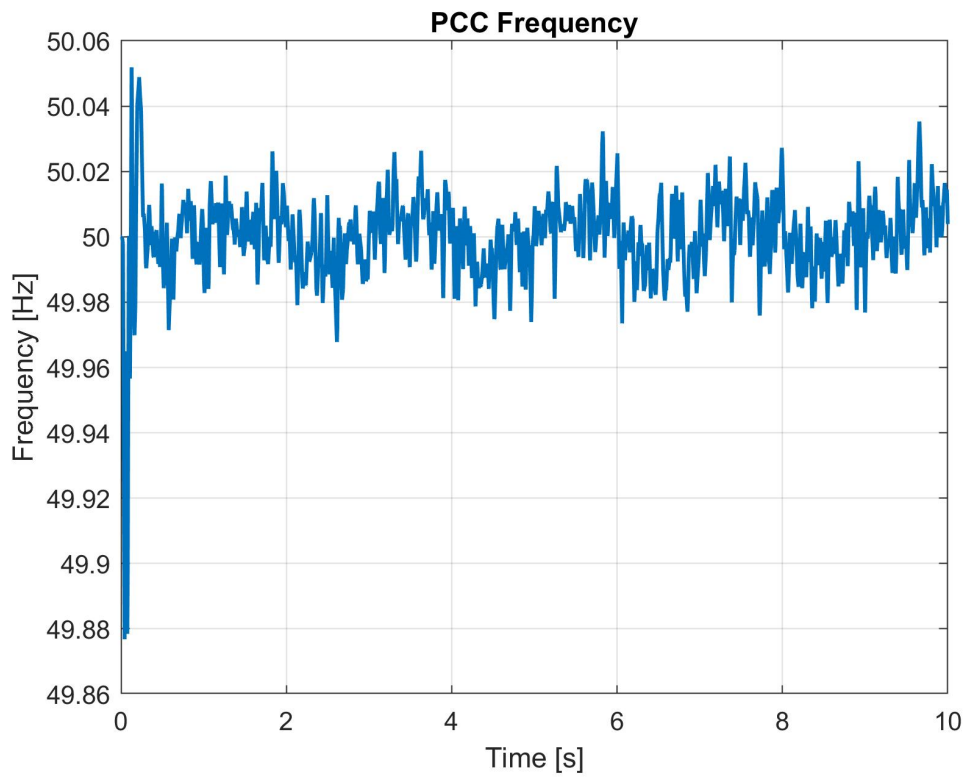


Figure B.2: Frequency behavior

Additional Case study B

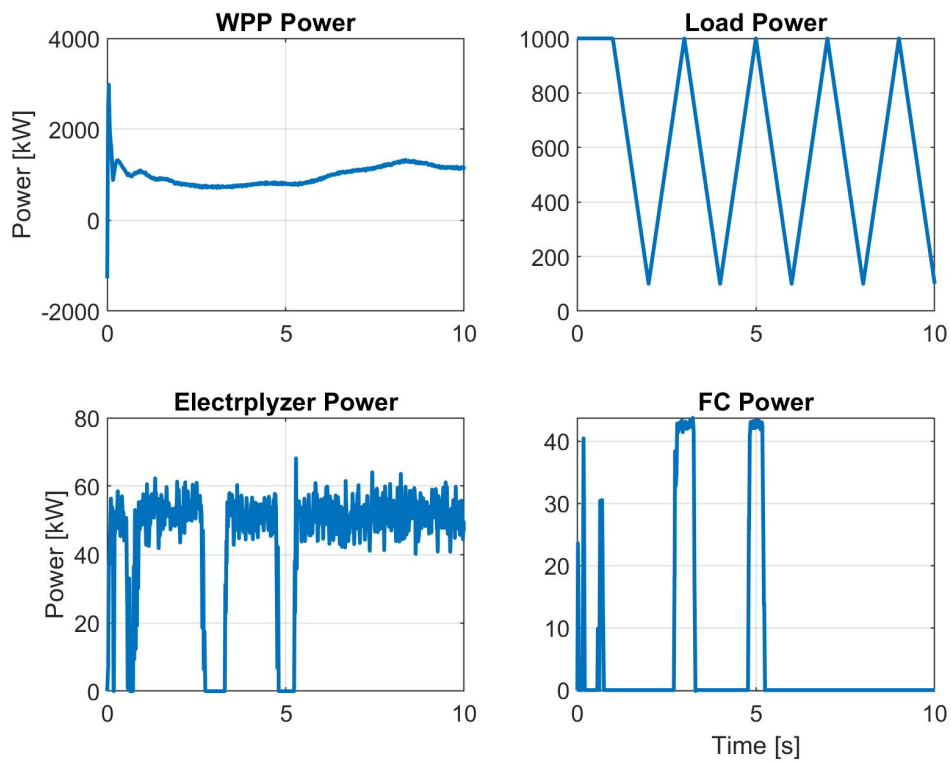


Figure B.3: Power profiles

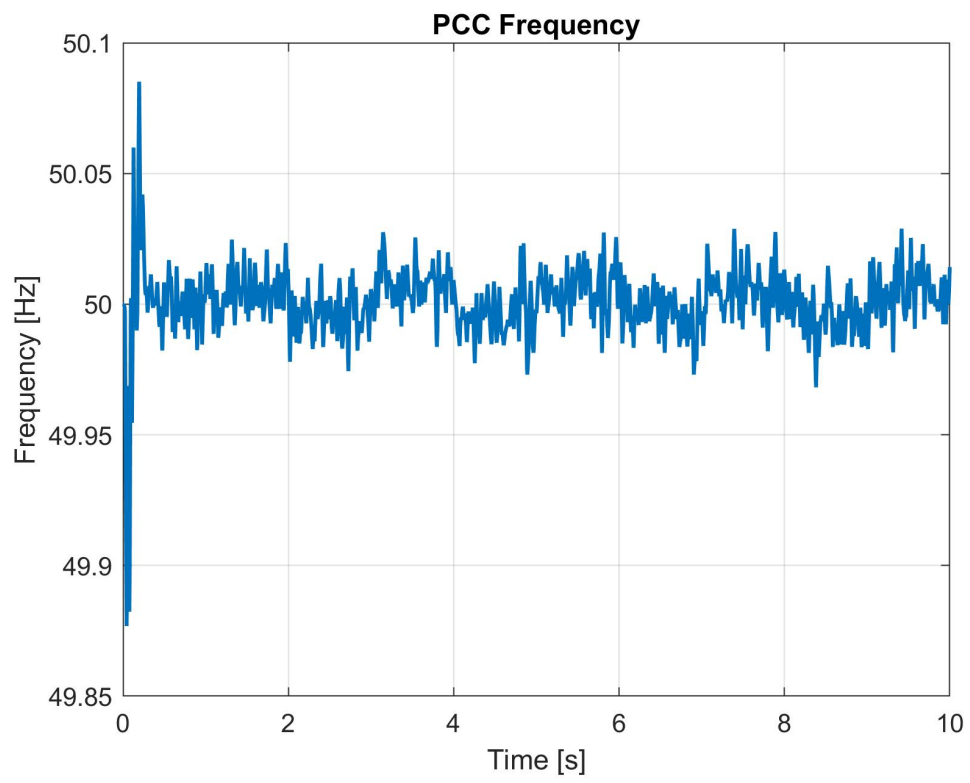


Figure B.4: Frequency behavior

Appendix C

Appendix C

The proposed system has been implemented in the OPAL-RT platform in order to conduct real-time assessments, but due to time limitations, the control algorithm has not been implemented in the system. Therefore, results could be shown after submitting the thesis.

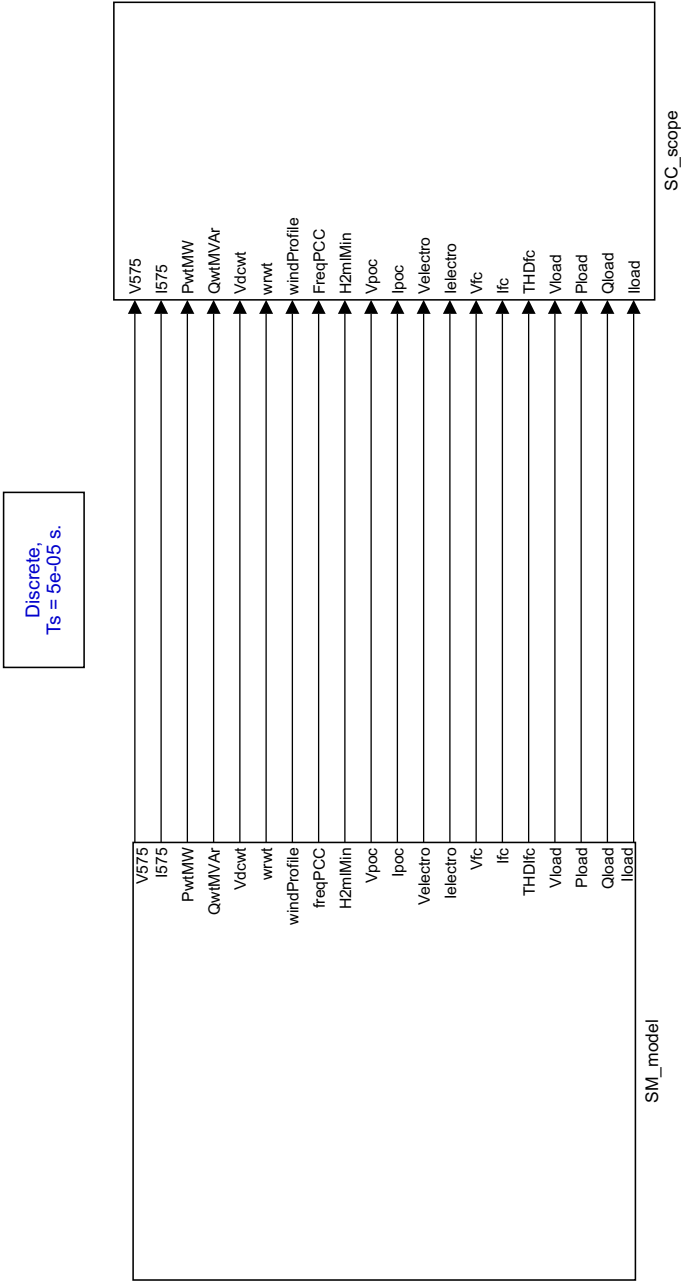


Figure C.1: Total system implementation in OPAL-RT

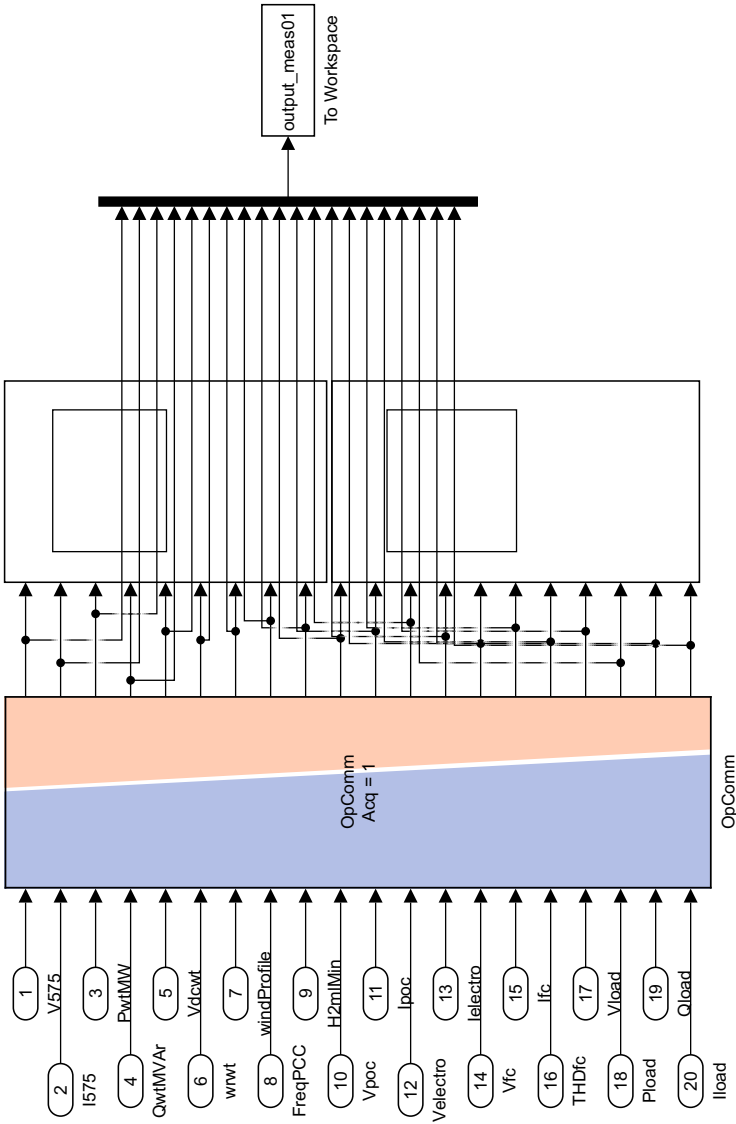


Figure C.3: Monitoring block and data acquisition in OPAL-RT